



1 Cold-water corals and hydrocarbon-rich seepage in the 2 Pompeia Province (Gulf of Cádiz) — living on the edge

3 Blanca Rincón-Tomás¹, Jan-Peter Duda^{2,3}, Luis Somoza⁴, Javier González⁴, Dominik
4 Schneider¹, Teresa Medialdea⁴, Pedro Madureira⁵, Michael Hoppert¹, and Joachim Reitner^{2,3}

5 ¹Georg-August-University Göttingen, Institute of Microbiology and Genetics, Grisebachstraße 8, 37077
6 Göttingen, Germany

7 ²Georg-August-University Göttingen, Göttingen Centre of Geosciences, Goldschmidtstraße 3, 37077 Göttingen,
8 Germany

9 ³Göttingen Academy of Sciences and Humanities, Theaterstraße 7, 37073 Göttingen, Germany

10 ⁴Marine Geology Dept., Geological Survey of Spain, IGME, Ríos Rosas 23, 28003 Madrid, Spain

11 ⁵Estrutura de Missão para a Extensão da Plataforma Continental. Rua Costa Pinto 165, 2770-047 Paço de Arcos,
12 Portugal

13 *Correspondence to:* Blanca Rincón-Tomás (b.rincontomas@gmail.com)

14 **Abstract.** Azooxanthellate cold-water corals (CWCs) are globally widespread and have commonly been found in
15 areas of active fluid seepage. The relationship between the CWCs and these fluids, however, is not well understood.
16 This study aims at unravelling the relationship between CWC development and hydrocarbon-rich seepage in the
17 Pompeia Province (Gulf of Cádiz, Atlantic Ocean). This region comprises mud volcanoes, coral ridges and fields
18 of coral mounds, which are all affected by the tectonically driven seepage of hydrocarbon-rich fluids. Rate and
19 type of seepage (i.e. focused, scattered, diffused, eruptive), however, is tightly controlled by a complex system of
20 faults and diapirs. Early diagenetic carbonates from the currently active Al Gacel MV exhibit $\delta^{13}\text{C}$ -signatures
21 down to -28.77‰ VPDB, indicating biologically derived methane as the main carbon source. The same samples
22 contained ^{13}C -depleted lipid biomarkers diagnostic for archaea such as crocetane ($\delta^{13}\text{C}$ down to -101.2‰ VPDB)
23 and PMI ($\delta^{13}\text{C}$ down to -102.9‰ VPDB), evidencing microbially mediated anaerobic oxidation of methane
24 (AOM). This is further supported by next generation DNA sequencing data, demonstrating the presence of AOM
25 related microorganisms (ANME archaea, sulfate-reducing bacteria) in the carbonate. Embedded corals in some of
26 the carbonates and CWC fragments exhibit less negative $\delta^{13}\text{C}$ values (-8.08 to -1.39‰ VPDB), pointing against
27 the use of methane as carbon source. Likewise, the absence of DNA from methane- and sulfide-oxidizing microbes
28 in a sampled coral does not support a chemosynthetic lifestyle of these organisms. In the light of these findings, it
29 appears that the CWCs benefit rather indirectly from hydrocarbon-rich seepage by using methane-derived
30 authigenic carbonates as substratum for colonization. At the same time, chemosynthetic organisms at active sites
31 prevent coral dissolution and necrosis by feeding on the seeped fluids (i. e. methane, sulfate, hydrogen sulfide),
32 allowing cold-water corals to colonize carbonates currently affected by hydrocarbon-rich seepage.

33 1. Introduction

34 Cold-water corals (CWCs) are a widespread, non-phylogenetic group of cnidarians which include hard skeleton
35 scleractinian corals, soft-tissue octocorals, gold corals, black corals and hydrocorals (Roberts et al., 2006; Roberts
36 et al., 2009; Cordes et al., 2016). They typically thrive at low temperatures ($4 - 12\text{ °C}$) and occur in water depths
37 of ca. $50 - 4000\text{ m}$. CWCs are azooxanthellate and solely rely on their nutrition as energy and carbon sources
38 (Roberts et al., 2009). Some scleractinian corals (e.g. *Lophelia pertusa*, *Madrepora oculata*, *Dendrophyllia*



39 *cornigera*, *Dendrophyllia alternata*, *Eguchipsammia cornucopia*) are able to form colonies or even large carbonate
40 mounds (Rogers et al., 1999; Wienberg et al., 2009; Watling et al., 2011; Somoza et al., 2014). Large vertical
41 mounds and elongated ridges formed by episodic growth of scleractinian corals (mainly *Lophelia pertusa*) are for
42 instance widely distributed along the continental margins of the Atlantic Ocean (Roberts et al., 2009). These
43 systems are of great ecological value since they offer sites for resting-, breeding-, and feeding for various
44 invertebrates and fishes (Cordes et al., 2016 and references therein).

45 Several ecological forces are discussed to control the initial settling, growth, and decline of CWCs. These include,
46 among others, an availability of suitable substrates for coral larvae settlement, low sedimentation rates,
47 oceanographic boundary conditions (e.g. salinity, temperature and density of the ocean water) and a sufficient
48 supply of nutrients through topographically controlled currents systems (e.g. Freiwald et al., 1999, 2002;
49 Mortensen et al., 2001; Roberts et al., 2003; Thiem et al., 2006; Dorschel et al., 2007; Dullo et al., 2008; Frank et
50 al., 2011; Van Rooij et al., 2011; Hebbeln et al., 2016). Alternatively, CWC ecosystems may be directly fueled
51 by fluid seepage, providing a source of e.g. sulfur compounds, nitrogen compounds, P, CO₂ and/or hydrocarbons
52 (Hovland, 1990; Hovland and Thomsen, 1997; Hovland et al., 1998). This relationship is supported by the common
53 co-occurrence of CWC-mounds and hydrocarbon-rich seeps around the world as e.g. at the Hikurangi Margin in
54 New Zealand (Liebetrau et al., 2010), the Brazil margin (e.g. Gomes-Sumida et al., 2004), the Darwin Mounds in
55 the northern Rockall Trough (Huvonne et al., 2009), the Kristin field on the Norwegian shelf (Hovland et al.,
56 2012), the western Alborán Sea (Margreth et al., 2011), and the Gulf of Cádiz (e.g. Díaz-del-Río et al., 2003;
57 Foubert et al., 2008). However, CWCs may also benefit rather indirectly from seepage. For instance, methane-
58 derived authigenic carbonates (MDACs) formed through the microbially mediated anaerobic oxidation of methane
59 (AOM; Suess & Whiticar, 1989; Hinrichs et al., 1999; Thiel et al., 1999; Boetius et al., 2000; Hinrichs & Boetius,
60 2002; Valentine, 2002; Boetius & Suess, 2004) potentially provide hard substrata for larval settlement (e.g. Díaz-
61 del-Río et al., 2003; Van Rooij et al., 2011; Magalhães et al. 2012; Le Bris et al., 2016; Rueda et al., 2016). On the
62 other hand, larger hydrocarbon-rich seepage related structures such as mud volcanoes and carbonate mud mounds
63 act as morphological barriers favoring turbulent water currents that deliver nutrients to the corals (Roberts et al.,
64 2009; Wienberg et al., 2009; Margreth et al., 2011; Vandrope et al., 2016).

65 In the Gulf of Cádiz, most CWC occurrences are “coral graveyards” (i.e., with only few living corals) that are
66 situated along the Iberian and Moroccan margins. These CWC systems are typically associated with diapiric
67 ridges, steep fault-controlled escarpments, and mud volcanoes (MVs) such as the Faro MV, Hesperides MV,
68 Mekness MV, and MVs in the Pen Duick Mud Volcano Province (Foubert et al., 2008; Wienberg et al., 2009).
69 MVs (and other conspicuous morphological structures in this region such as pockmarks) are formed through
70 tectonically induced fluid flow (Pinheiro et al., 2003; Somoza et al., 2003; Medialdea et al., 2009; León et al.,
71 2010; 2012). This is because of the high regional tectonic activity and high fluid contents of sediments in this area
72 (mainly CH₄ and, to a lesser extent, H₂S, CO₂, and N₂; Pinheiro et al., 2003; Hensen et al., 2007; Scholz et al.,
73 2009; Smith et al., 2010; González et al., 2012). However, the exact influence of fluid flow on CWC growth in
74 this region remains elusive.

75 This study aims at elucidating the linkage between the present-day formation of MDACs and CWCs development
76 along the Pompeia Province (**Fig. 1**), which englobes mud volcanoes as the Al Gacel MV (León et al., 2012),
77 diapiric coral ridges and mounds. We address this question by the combined analysis of high-resolution ROV
78 underwater images, geophysical data (e.g. seabed topography, deep high-resolution multichannel seismic
79 reflection data), and sample materials (petrographic features, δ¹³C- and δ¹⁸O-signatures of carbonates, lipid



80 biomarkers and environmental 16s rDNA sequences of the prokaryotic microbial community). Based on our
81 findings, we propose an integrated model to explain the tempo-spatial and genetic relations between CWCs,
82 chemosynthetic fauna and hydrocarbon-rich seepage in the study area.

83 2. Materials and Methods

84 This study is based on collected data from the Pompeia Province, during the Subvent-2 cruise in 2014 aboard the
85 R/V Sarmiento de Gamboa. The analyzed samples were recovered from the Al Gacel MV (D10-R3, D10-R7, D11-
86 R8) and the Northern Pompeia Coral Ridge (D03-B1) (**Fig. 1**).

87 2.1. Geophysical survey

88 Seabed topography of the studied sites was mapped by using an Atlas Hydrosweep DS (15 kHz and 320 beams)
89 multibeam echosounder (MBES). Simultaneously, ultra-high resolution sub-bottom profiles were acquired with
90 an Atlas Parasound P-35 parametric chirp profiler (0.5 – 6 kHz). Deep high-resolution multichannel seismic
91 reflection data was obtained using an array of 7 SERCEL gi-guns (system composed of 250 + 150 + 110 + 45
92 cubic inches) with a total of 860 cubic inches. The obtained data were recorded with an active streamer
93 (SIG®16.3x40.175; 150 m length with 3 sections of 40 hydrophones each). The shot interval was 6 seconds and
94 the recording length 5 seconds two-way travel time (TWT). Data processing (filtering and stacking) was performed
95 on board with Hot Shots software.

96 2.2. Video survey and analysis

97 A remotely operated vehicle (ROV-6000 Luso) was used for photographic documentation (high definition digital
98 camera, 1024x1024 pixel) and sampling. The ROV was further equipped with a STD/CTD-SD204 sensor (*in-situ*
99 measurements of salinity, temperature, oxygen, conductivity, sound velocity and depth), HydroC™ sensors (*in-*
100 *situ* measurements of CO₂ and CH₄) and Niskin bottles (CH₄ concentrations).

101 2.3. Petrographic analysis

102 General petrographic analysis was performed on thin sections (ca. 60 μm thickness) with a Zeiss SteREO
103 Discovery.V8 stereomicroscope (transmitted- and reflected light) linked to an AxioCam MRc 5-megapixel camera.
104 Additional detailed petrographic analysis of textural and mineralogical features was conducted on polished thin
105 sections (ca. 30 μm thickness) using a DM2700P Leica Microscope coupled to a DFC550 digital camera.
106 Carbonate textures have been classified following Dunham (1962) and Embry & Klovan (1971).

107 2.4. Stable isotopes ($\delta^{13}\text{C}$, $\delta^{18}\text{O}$) of carbonates

108 Stable carbon and oxygen isotope measurements were conducted on ca. 0.7 mg carbonate powder obtained with a
109 high precision drill (ø 0.8 mm). The analyses were performed with a Thermo Scientific Kiel IV carbonate device
110 coupled to a Finnigan Delta Plus gas isotope mass spectrometer. Reproducibility was checked through the replicate
111 analysis of a standard (NBS19) and was generally better than 0.1 ‰. Stable carbon and oxygen isotope values are
112 expressed in the standard δ notation as per mill (‰) deviations relative to Vienna Pee Dee Belemnite (VPDB).

113 2.5. Lipid biomarker analysis



114 2.5.1. Sample preparation

115 All materials used were pre-combusted (500 °C for >3 h) and/or extensively rinsed with acetone prior to sample
116 contact. A laboratory blank (pre-combusted sea sand) was prepared and analyzed in parallel to monitor laboratory
117 contaminations.

118 The preparation and extraction of lipid biomarkers was conducted in orientation to descriptions in Birgel et al.
119 (2006). Briefly, the samples were first carefully crushed with a hammer and internal parts were powdered with a
120 pebble mill (Retsch MM 301, Haan, Germany). Hydrochloric acid (HCl; 10 %) was slowly poured on the powdered
121 samples which were covered with dichloromethane (DCM)-cleaned water. After 24 h of reaction, the residues (pH
122 3 – 5) were repeatedly washed with water and then lyophilized.

123 3 g of each residue was saponified with potassium hydroxide (KOH; 6 %) in methanol (MeOH). The residues were
124 then extracted with methanol (40 mL, 2x) and, upon treatment with HCl (10 %) to pH 1, in DCM (40 mL, 2x) by
125 using ultra-sonification. The combined supernatants were partitioned in DCM vs. water (3x). The total organic
126 extracts (TOEs) were dried with sodium sulfate (NaSO₄) and evaporated with a gentle stream of N₂ to reduce loss
127 of low-boiling compounds (cf. Ahmed and George, 2004).

128 50 % of each TOE was separated over a silica gel column (0.7 g Merck silica gel 60 conditioned with *n*-hexane;
129 1.5 cm i.d., 8 cm length) into (a) hydrocarbon (6 mL *n*-hexane), (b) alcohol (7 mL DCM/acetone, 9:1, v:v) and (c)
130 carboxylic acid fractions (DCM/MeOH, 3:1, v:v). Only the hydrocarbons were subjected to gas chromatography–
131 mass spectrometry (GC-MS).

132 2.5.2. Gas chromatography–mass spectrometry (GC-MS)

133 Lipid biomarker analyses of the hydrocarbon fraction were performed with a Thermo Scientific Trace 1310 GC
134 coupled to a Thermo Scientific Quantum XLS Ultra MS. The GC was equipped with a capillary column
135 (Phenomenex Zebron ZB-5MS, 30 m length, 250 µm inner diameter, 0.25 µm film thickness). Fractions were
136 injected into a splitless injector and transferred to the column at 300 °C. The carrier gas was He at a flow rate of
137 1.5 mL min⁻¹. The GC oven temperature was ramped from 80°C (1 min) to 310 °C at 5 °C min⁻¹ (held for 20 min).
138 Electron ionization mass spectra were recorded in full scan mode at an electron energy of 70 eV with a mass range
139 of *m/z* 50 – 600 and scan time of 0.42 s. Identification of individual compounds was based on comparison of mass
140 spectra and GC retention times with published data and reference compounds.

141 2.5.3 Gas chromatography–combustion–isotope ratio mass spectrometer (GC-C-IRMS)

142 Compound specific δ¹³C analyses were conducted with a Trace GC coupled to a Delta Plus IRMS via a
143 combustion-interface (all Thermo Scientific). The combustion reactor contained CuO, Ni and Pt and was operated
144 at 940°C. The GC was equipped with two serially linked capillary columns (Agilent DB-5 and DB-1; each 30 m
145 length, 250 µm inner diameter, 0.25 µm film thickness). Fractions were injected into a splitless injector and
146 transferred to the GC column at 290°C. The carrier gas was He at a flow rate of 20 ml min⁻¹. The temperature
147 program was identical to the one used for GC-MS (see above). CO₂ with known δ¹³C value was used for internal
148 calibration. Instrument precision was checked using a mixture of *n*-alkanes with known isotopic composition.
149 Carbon isotope ratios are expressed as δ¹³C (‰) relative to VPDB.

150 2.6. Amplicon sequencing of 16S rRNA genes



151 2.6.1. DNA extraction and 16S rRNA gene amplification

152 About 1 – 4 g of solid samples were first mashed with mortar and liquid nitrogen to fine powder. Three biological
153 replicates were used per sample. Total DNA was isolated with a Power Soil DNA Extraction Kit (MO BIO
154 Laboratories, Carlsbad, CA). All steps were performed according to the manufacturer's instructions.

155 Bacterial amplicons of the V3 – V4 region were generated with the primer set MiSeq_Bacteria_V3_forward
156 primer (5'-TCGTCGGCAGCGTCAGATGTGTATAAGAGACAGCCTACGGGNGGCWGCAG-3') and
157 MiSeq_Bacteria_V4_reverse primer (5'-
158 GTCTCGTGGGCTCGGAGATGTGTATAAGAGACAGGACTACHVGGGTATCTAATCC-3'). Likewise,
159 archaeal amplicons of the V3 – V4 region were generated with the primer set MiSeq_Archaea_V3_forward primer
160 (5'-TCGTCGGCAGCGTCAGATGTGTATAAGAGACAG-GGTGBCAGCCGCCGCGTAA-3') and
161 MiSeq_Archaea_V4_reverse primer (5'-GTCTCGTGGGCTCGGAGATGTGTATAAGAGACAG-
162 CCCCCAATTYCTTTAAG-3'). 50 µl of the PCR reaction mixture for bacterial DNA amplification, contained
163 1 U Phusion high fidelity DNA polymerase (Biozym Scientific, Oldendorf, Germany), 5% DMSO, 0.2 mM of
164 each primer, 200 µM dNTP, 0.15 µl of 25 mM MgCl₂, and 25 ng of isolated DNA. The PCR protocol for bacterial
165 DNA amplification included (i) initial denaturation for 1 min at 98 °C, (ii) 25 cycles of 45 s at 98 °C, 45 s at 60 °C,
166 and 30 s at 72 °C, and (iii) a final extension at 72 °C for 5 min. The PCR reaction mixture for archaeal DNA
167 amplification was similarly prepared but contained instead 1 µl of 25 mM MgCl₂ and 50 ng of isolated DNA. The
168 PCR protocol for archaeal DNA amplification included (i) initial denaturation for 1 min at 98 °C, (ii) 10 cycles of
169 45 s at 98 °C, 45 s at 63 °C, and 30 s at 72 °C, (iii) 15 cycles of 45 s at 98 °C, 45 s at 53 °C, and 30 s at 72 °C, and
170 (iv) a final extension at 72 °C for 5 min.

171 PCR products were checked by agarose gel electrophoresis and purified using the GeneRead Size Selection Kit
172 (QIAGEN GmbH, Hilden, Germany).

173 2.6.2. Data analysis and pipeline

174 Illumina PE sequencing of the amplicons and further process of the sequence data were performed in the Göttingen
175 Genomics Laboratory (Göttingen, Germany). After Illumina MiSeq processing, sequences were analyzed as
176 described in Egelkamp et al. (2017) with minor modifications. In brief, paired-end sequences were merged using
177 PEAR v0.9.10 (Zhang et al., 2014), sequences with an average quality score below 20 and containing unresolved
178 bases were removed with QIIME 1.9.1 (Caporaso et al., 2010). Non-clipped reverse and forward primer sequences
179 were removed by employing cutadapt 1.15 (Martin, 2011). USEARCH version 9.2.64 was used following the
180 UNOISE pipeline (Edgar, 2010). In detail, reads shorter than 380 bp were removed, dereplicated, and denoised
181 with the UNOISE2 algorithm of USEARCH resulting in amplicon sequence variants (ASVs) (Callahan et al.,
182 2017). Additionally, chimeric sequences were removed using UCHIME2 in reference mode against the SILVA
183 SSU database release 132 (Yilmaz et al., 2014). Merged paired-end reads were mapped to chimera-free ASVs and
184 an abundance table was created using USEARCH. Taxonomic classification of ASVs was performed with BLAST
185 against the SILVA database 132. Extrinsic domain ASVs, chloroplasts, and unclassified ASVs were removed from
186 the dataset. Sample comparisons were performed at same surveying effort, utilizing the lowest number of
187 sequences by random subsampling (20,290 reads for bacteria, 13,900 reads for archaea).

188 The paired-end reads of the 16S rRNA gene sequencing were deposited in the National Center for Biotechnology
189 Information (NCBI) in the Sequence Read Archive SRP156750.



190 3. Results

191 3.1. The Pompeia Province — geological settings

192 The Pompeia Province is situated in the Gulf of Cádiz offshore Morocco, within the so-called Middle Moroccan
193 Field (Ivanov et al., 2000) at water-depths between 860 and 1000 m (**Fig. 1**). It comprises the active Al Gacel
194 MV (**Fig. 1, C**), another mud volcano which is extinct (further referred as extinct MV) and two east-west elongated
195 ridges (Northern Pompeia Coral Ridge and Southern Pompeia Coral Ridge). Scattered coral-mounds surround the
196 ridges with a smooth relief (**Fig. 1, B**). CWCs were observed on seismic profiles resting on all these morphological
197 features. Detailed geological profiles and 3D images of these features are shown in **Figs. 2** and **3**.

198 The Al Gacel MV is a cone-shape structure, 107 m high and 944 m wide, with its summit at 762 m depth and
199 surrounded by a 11 m deep rimmed depression (León et al., 2012) (**Fig. 1, C**). It is directly adjacent to the Northern
200 Pompeia Coral Ridge (**Fig. 2, A–B**), which extends ca. 4 km in westward direction (**Fig. 2, A–B**) and it is
201 terminated by the Pompeia Escarpment (**Fig. 1, B; Fig. 2, C**). High resolution seismic profiles of the Pompeia
202 Escarpment show CWC build-ups (R1 to R4) with steep lateral scarps of ca. 40 m height (**Fig. 2, C**). This MV is
203 of sub-circular shape and exhibits a crater at its top (**Fig. 2, A–B**).

204 Ultra-high resolution sub-bottom seismic profile crossing the Pompeia Province from northwest (NW) to southeast
205 (SE) (**Fig. 3, A**), shows (i) the Al Gacel MV surrounded by bottom-current deposits, (ii) an up to 130 m high CWC
206 framework, growing on top the Southern Pompeia Coral Ridge, and (iii) semi-buried CWC mounds surrounding
207 the ridge in areas of low relief. These CWC mounds locally form smooth, up to 25 – 30 m high top-rounded reliefs
208 that are exposed, but then taper downward below the seafloor (applying sound speeds of 1750 m/s in recent
209 sediments). Additionally, a multichannel seismic profile following the same track but with higher penetration
210 below the seafloor (**Fig. 3, B**) shows high amplitude reflections inside the Al Gacel cone and enhanced reflections
211 at the top of the diapirs (yellow dotted-line in **Fig. 3, B**), pointing to the occurrence of gas (hydrocarbon)-charged
212 sediments. It furthermore exhibits breaks in seismic continuity and diapiric structures at different depths below the
213 Southern Pompeia Coral Ridge and the Al Gacel MV, evidencing a fault system (**Fig. 3, B**). These tectonic
214 structures may promote the development of overpressure areas (OP in **Fig. 3, B**) and consequent upward fluid flow
215 to the surface.

216 3.2. ROV observation and measurements

217 Submersible ROV surveys at the Al Gacel MV (**Fig. 1, C**) revealed the presence of dispersed pockmark
218 depressions at the eastern (Dive 10, 790 m) and northern flanks (Dive 11, 760 – 825 m depth). These sites are
219 characterized by focused but low intensity seafloor bubbling (e.g. **Fig. 4, B; Fig. 5, A**). Analysis of water samples
220 revealed CH₄-concentration up to 171 nM during Dive 10 and up to 192 nM during Dive 11 (Sánchez-Guillamón
221 et al., 2015). Pockmarks were essentially formed by grey-olive mud breccia sediments and characterized by
222 deposits of authigenic carbonates appearing in the center and edges, together with typical methane-seep related
223 organisms (e.g. sulfide-oxidizing bacterial mats, chemosynthetic bivalves, siboglinid tubeworms) (**Fig. 4, B–C;**
224 **Fig. 5**). Communities of non-chemosynthetic organisms (e.g. sponges, corals) were also found at pockmarks (**Fig.**
225 **4, B–C; Fig. 5, C**), but were more abundant in places where no seepage was detected (**Fig. 4, A**).

226 Observations with the submersible ROV at the Northern Pompeia Coral Ridge and the extinct MV (Dive 03)
227 revealed widespread and abundant occurrences of dead scleractinian-corals (mainly *Madrepora oculata* and
228 *Lophelia pertusa*) currently colonized by few non-chemosynthetic organisms (e.g. *Corallium tricolor*, other



229 octocorals, sea urchins) (**Fig. 6, B–D**). Locally, grey-black colored patches of sulfide-oxidizing bacterial mats
230 surrounded by dead chemosynthetic bivalves (*Lucinoma asapeus* and *Thysira vulcolutre*) were detected (**Fig. 6,**
231 **A**). CH₄-seepage appeared to be less than at the Al Gacel MV, with concentrations of 80 – 83 nM.
232 Water parameters display homogenous values between the four sampling sites (10 °C temperature, ca. 52 – 55 %
233 dissolved oxygen, ca. 31 Kg/m³ density) (**Table 1**).

234 3.3. Petrography and stable isotopes signatures of carbonates ($\delta^{18}\text{O}$, $\delta^{13}\text{C}$)

235 Sample D10-R3 derives from a field of carbonates at the base of the Al Gacel MV which is inhabited by sponges
236 and corals (**Fig. 4, A**). The sample is a frammestone composed of deep water scleractinian corals (*Madrepora* and
237 rare *Lophelia*) (**Fig. 7, A–B**). The corals are typically cemented by microbial automicrite (*sensu* Reitner et al.
238 1995) followed by multiple generations of aragonite. A matrix of dark allomicrite (*sensu* Reitner et al. 1995) with
239 oxidized framboidal pyrites and remains of planktonic foraminifera is restricted to few bioerosional cavities (ca.
240 5%) in the skeletons of dead corals (**Fig. 8, A–B**). $\delta^{13}\text{C}$ signatures of the matrix and cements range from –26.68 to
241 –18.38 ‰, while the embedded coral fragments exhibit $\delta^{13}\text{C}$ values between –5.58 and –2.09 ‰ (**Fig. 7, B; Table**
242 **2**). The $\delta^{18}\text{O}$ values generally range from +2.35 to +3.92 ‰ (**Fig. 9; Table 2**).

243 Sample D10-R7 was recovered from a pockmark on the eastern site of the Al Gacel MV that is virtually influenced
244 by active seepage (**Fig. 3, C**). It consists of black carbonate and exhibits a strong hydrogen sulfide (H₂S) odor (**Fig.**
245 **5, B; Fig. 7, C–D**). The top of this sample was inhabited by living octocorals (**Fig. 5, C**), while chemosymbiotic
246 siboglinid worms were present on the lower surface (**Fig. 5, D**). The sample is characterized by a grey peloidal
247 wackestone texture consisting of allomicrite with abundant planktonic foraminifers and few deep water miliolids.
248 The sample furthermore exhibits some fractured areas which are partly filled by granular and small fibrous cement,
249 probably consisting of Mg-calcite. Locally, light brownish crusts of microbial automicrite similar to ones in D10-
250 R3 are present (see above). Framboidal pyrite is abundant and often arranged in aggregates (**Fig. 8, C–D**). The
251 carbonate exhibits $\delta^{13}\text{C}$ values ranging from –28.77 to –21.13 ‰ and $\delta^{18}\text{O}$ values from +2.37 to +3.15 ‰ (**Fig. 9;**
252 **Table 2**).

253 Sample D11-R8 stems from an area with meter-sized carbonate blocks at the summit of the Al Gacel MV and is
254 mainly colonized by sponges and worms (**Fig. 4, D**). The sample generally exhibits a light grey mud- to wackestone
255 texture consisting of allomicrite with few scleractinian-coral fragments and planktonic foraminifers (**Fig. 7, E–F**).
256 The carbonate furthermore contains abundant quartz silt and, locally, pyrite enrichments. A further prominent
257 feature are voids that are encircled by dark grey halos and exhibit brownish margins (due to enrichments of very
258 small pyrite crystals and organic matter, respectively). $\delta^{13}\text{C}$ signatures of the matrix and cements range from
259 –14.82 to –14.74 ‰, while embedded coral fragments exhibit $\delta^{13}\text{C}$ values of –4.91 to –2.99 ‰ (**Fig. 7, F; Table**
260 **2**). $\delta^{18}\text{O}$ values generally range from +1.49 to +5.60 ‰ (**Fig. 9; Table 2**).

261 Sample D03-B1 is a necrotic fragment of a living scleractinian coral (*Madrepora oculata*) recovered from the
262 Northern Pompeia Coral Ridge (**Fig. 6, D; Fig. 7, G**). The coral-carbonate exhibits $\delta^{13}\text{C}$ values ranging from –8.08
263 to –1.39 ‰ and $\delta^{18}\text{O}$ values from –0.31 to +2.26 ‰ (**Fig. 9; Table 2**).

264 3.4. Lipid biomarkers and compound specific carbon isotope signatures

265 The hydrocarbon fractions of the sample D10-R7 mainly consist of the irregular, tail-to-tail linked acyclic
266 isoprenoids 2,6,11,15-tetramethylhexadecane (C₂₀; crocetane), 2,6,10,15,19-pentamethylcosane (C₂₅; PMI), as



267 well as of several unsaturated homologues of these compounds (**Fig. 10**). Additionally, it contains the regular,
268 head-to-tail linked acyclic isoprenoid pristane (C₁₉) and the cyclic isoprenoid hop-17(21)-ene.
269 The hydrocarbon fraction of sample D11-R8 is dominated by *n*-alkanes with chain-lengths ranging from C₁₄ to
270 C₂₈ (maxima at *n*-C₁₆ and, subordinated, at *n*-C₂₀ and *n*-C₂₈) (**Fig. 10**). The sample further contains pristane,
271 crocetane, the head-to-tail linked acyclic isoprenoid phytane (C₂₀) and traces of PMI.
272 Crocetane and PMI exhibited strongly depleted $\delta^{13}\text{C}$ values in sample D10-R7 (−101.2 ‰ and
273 −102.9 ‰, respectively), while they showed less depleted $\delta^{13}\text{C}$ values in sample D11-R8 (−57.2 ‰ and −74.3 ‰,
274 respectively). $\Delta^{13}\text{C}$ values of *n*-alkanes in sample D11-R8 (*n*-C₁₇₋₂₂) ranged between −30.8 ‰ and −33.0 ‰ (**Table**
275 **3**).

276 3.5. DNA inventories (MiSeq Illumina sequences)

277 Bacterial DNA (**Fig. 11, A**) from samples D10-R3 (authigenic carbonate, base of the Al Gacel MV) and D03-B1
278 (*Madrepora oculata* fragment, Northern Pompeia Coral Ridge) mainly derives from taxa that typically thrive in
279 the water-column (e. g. Actinobacteria, Acidobacteria, Chloroflexi, Bacteroidetes, Woeseiaceae, Dadabacteria,
280 Kaiserbacteria, Poribacteria, Planctomycetes, Gemmatimonadetes). The sample D10-R3 furthermore contains
281 bacterial DNA of the nitrite-oxidizing bacteria *Nitrospira sp.*, while the sample D03-B1 contains DNA of the
282 bacterial taxa Verrucomicrobia, Enterobacteria, *Nitrosococcus*. Noteworthy, one amplicon sequence variant
283 (ASV_189) with low number of clustered sequences has been found in D03-B1, identified as a methanotrophic
284 symbiont of *Bathymodiolus mauritanicus* (see Rodrigues et al., 2013).

285 Up to 50 % of bacterial DNA in sample D10-R7 (authigenic carbonate, top of the Al Gacel MV) derives from taxa
286 that are commonly associated with fluid seepage and AOM, i.e. sulfide-oxidizing bacteria, sulfate-reducing
287 bacteria (SRB) and methane-oxidizing bacteria. The most abundant are SRB taxa like SEEP-SRB1, SEEP-SRB2,
288 *Desulfatiglans*, *Desulfobulbus* and *Desulfococcus*, which typically form consortia with ANME archaea.

289 Archaeal DNA (**Fig. 11, B**) from samples D10-R3 and D03-B1 mainly consist of *Cenarchaeum sp.*, which
290 represents 70 – 90 %. *Candidatus Nitrosopumilus* is the second most abundant in both samples, representing 5 –
291 20 %. On the contrary, around 90 % of archaeal DNA in D10-R7 is related to ANME-1 and ANME-2 groups, in
292 good concordance with the relative abundances of SRB DNA.

293 Details of the number of reads per taxa are shown in the supplementary data, **Tables 1** and **2**.

294 4. Discussion

295 4.1. Evidence of hydrocarbon-rich seepage affecting the Pompeia Province

296 2D multichannel-seismic images show that the Pompeia Province is affected by fluid expulsion related to
297 compressional diapiric ridges and thrust faults (**Fig. 3, B**), as it has been reported from other areas of the Gulf of
298 Cádiz (Somoza et al., 2003; Van Rensbergen et al., 2005; Medialdea et al., 2009). There seem to be different types
299 of fault-conduit systems that link the overpressure zones (OP) with the seafloor (**Fig. 3, B**), controlling both type
300 and rate of seepage (e.g. eruptive, focused, diffused or dripping-like). At the Al Gacel MV, conduits are for
301 instance mainly linked to faults and a dense hydro-fracture network, allowing the migration of hydrocarbon-rich
302 muds from the overpressure zone to the surface. During active episodes, eruptions lead to the formation of mud-
303 breccia flows as observed in gravity cores (e.g. León et al., 2012). During rather dormant episodes, focused and
304 dripping-like seepage predominates, forming pockmark features (**Fig. 4, B**).



305 Currently, the Al Gacel MV is affected by continuous and focused dripping-like seepages. These sites of active
306 seepage are characterized by carbonates that are suspected to be methane-derived (e.g. sample D10-R7, **Fig. 4, B–**
307 **C**). In-situ ROV-measurements and subsequent water sample analysis demonstrated high proportions of CH₄ in
308 fluids that were escaping upon removal of the D10-R7 carbonate (171 nM; **Fig. 5, A**) (Sánchez-Guillamón et al.,
309 2015). This association suggests a genetic relationship between hydrocarbon-rich seepage and the carbonate, as
310 also evidenced by the low $\delta^{13}\text{C}$ -values of the carbonates analyzed herein (down to ca. -30‰ , **Fig. 9; Table 2**).
311 Indeed, the grey peloidal texture of this sample resembles that of AOM-derived automicrites from the Black Sea
312 that are related to micro-seepage of methane (cf. Reitner et al., 2005). The here observed isotopically depleted
313 acyclic isoprenoids such as crocetane and PMI ($\delta^{13}\text{C}$ values between ca. -103 and -57‰ ; **Fig. 10; Table 3**) are
314 typical fingerprints of AOM-associated Archaea (Hinrichs et al., 1999; Thiel et al., 1999, 2001; Peckmann et al.,
315 2001; Peckmann & Thiel, 2004), which is also in good accordance with the high abundance of DNA related to
316 ANME. At the same time, abundant framboidal pyrite in the carbonate (**Fig. 8, C–D**) and SRB-related DNA (**Fig.**
317 **11**) evidences microbial sulfate reduction in the environment. All these evidences clearly demonstrate that the
318 carbonates have been formed via AOM, fueled by fluids from the underlying mud diapir.

319 Other carbonate samples from the Al Gacel MV (i.e. D10-R3 and D11-R8) probably have also been formed due
320 to AOM as they are also isotopically depleted ($\delta^{13}\text{C}$ values between ca. -25 and -15‰ , **Fig. 9, Table 2**). However,
321 no active gas bubbling was observed during sampling, even though both samples still contain open voids which
322 could form pathways for a continuous migration of fluids. In fact, several characteristics of these voids (e.g. dark
323 halos formed by pyrite, brownish margins due to organic matter enrichments) are very similar to those of methane-
324 derived carbonate conduits (cf. Reitner et al., 2015). This could imply that the intensity of hydrocarbon-rich
325 seepage and consequently AOM, may have fluctuated through time. The relatively low dominance of crocetane
326 and PMI in sample D11-R8 (**Fig. 10**), as well as their moderately depleted $\delta^{13}\text{C}$ values (-57.2‰ and -74.3‰ ,
327 respectively; **Table 3**), could be due to mixing effects and thus be in good accordance varying intensities of AOM
328 in the environment. Also, the presence of only few AOM-related DNA sequences (**Fig. 11**) and partly oxidized
329 pyrites in sample D10-R3 (**Fig. 8, A–B**) are well in line with this scenario. In concert it appears that the seepage
330 intensity has indeed been fluctuating.

331 There is no evidence for eruptive extrusions of muddy materials at the coral ridges. In the Southern Pompeia Coral
332 Ridge (**Fig. 3**), diapirs appears to rather promote an upward migration of hydrocarbon-rich fluids in a divergent
333 way throughout a more extensive seabed area. This results in a continuous and diffused seepage, which promotes
334 the occurrence of AOM and the formation of MDACs at the base of the ridges, related to the sulphate-methane
335 transition zone (SMTZ) (Boetius et al., 2000; Hinrichs and Boetius, 2002; González et al., 2012a). This is in good
336 accordance with the detection of methane (80 – 83 nM) at the Northern Pompeia Coral Ridge and the presence of
337 sulfide-oxidizing bacterial mats and shells of dead chemosynthetic bivalves at the western part of the ridge (**Fig.**
338 **6, A**). Likewise, the CWC Mounds Field surrounding the Southern Pompeia Coral Ridge (**Fig. 3**) is thoroughly
339 characterized by micro-seeps, due to ascending fluids from OPs through low-angle faults. This type of focused
340 seepage may promote formation of MDAC pavements in deeper layers of the sediments (**Fig. 3**), similar to coral
341 ridges along the Pen Duick Escarpment (Wehrmann et al., 2011). The generation of MDAC-hotspots at sites of
342 such seepage also explain the geometry of the downward tapering cones (**Fig. 3**).

343 4.2. Ecological meaning of hydrocarbon-rich seepage for CWCs



344 Our data suggests contemporaneous micro-seepage and CWC growth in the Pompeia Province (e.g. **Fig. 4, B**).
345 This relationship has also been observed elsewhere, e.g. in North Sea and off Mid Norway (Hovland, 1990;
346 Hovland & Thomsen, 1997), and the Angola margin (Le Guilloux et al., 2009). However, scleractinian fragments
347 recovered from the Al Gacel MV (embedded in carbonates D10-R3 and D11-R8) and the Northern Pompeia Coral
348 Ridge (D03-B1, necrotic part of a living *Madrepora oculata*) displayed barely depleted $\delta^{13}\text{C}$ values (ca. -8 to -1
349 ‰; **Fig. 9; Table 2**), close to the $\delta^{13}\text{C}$ of marine seawater (0 ± 3 ‰, e.g. Hoefs, 2015). This does not support a
350 significant uptake of methane-derived carbon by the CWCs and thus a direct trophic dependency as previously
351 proposed (Hovland, 1990). Furthermore, the only DNA in sample D03-B1 that could be attributed to a potential
352 methanotrophic endosymbiont (ASV_189: Rodrigues et al., 2013) occurred in minor amounts and most likely
353 represents contamination from the environment or during sampling. Taken together, there is no evidence that
354 CWCs in the working area harbor microbial symbionts which potentially could utilize the hydrocarbon-rich fluids.
355 More likely, the CWCs feed on a mixture of phytoplankton, zooplankton and dissolved organic matter as
356 previously proposed for ones in other regions (Kiriakoulakis et al., 2005; Duineveld et al., 2007; Becker et al.,
357 2009; Liebetrau et al., 2010). This is in good accordance with the presence of DNA from various common archaeal
358 and bacterial taxa (e.g. Acidobacteria, Actinobacteria, Candidatus *Nitrosopumilus*, *Cenarchaeum sp.*) and some
359 potential members of the corals' holobiont (e.g. Enterobacteria, Verrucomicrobia, *Nitrosococcus sp.*) (Sorokin,
360 1995; Rådecker et al., 2015; Webster et al., 2016) in sample D03-B1 (**Fig. 11**).

361 CWC development and hydrocarbon-rich seepage are consequently linked *via* the formation of MDAC deposits,
362 which provide the hard substrata needed for CWC larval settlement (e.g. Díaz-del-Río et al., 2003; Van Rooij et
363 al., 2011; Magalhães et al., 2012; Le Bris et al., 2016; Rueda et al., 2016). If too severe, however, fluid flow and
364 associated metabolic processes can result in local conditions that are lethal to CWCs (see 4.3). Moreover, AOM
365 fueled by fluid flow can also cause an entombment of the CWCs by MDACs (Wienberg et al., 2009, Wienberg &
366 Titschack, 2015), as observed in D10-R3 and D11-R8 carbonates from the Al Gacel MV (**Figs. 7 and 9; Tabs. 2**
367 **and 3**). It is therefore not surprising that large CWC systems in the Pompeia Province are always linked to
368 structures that are affected by rather mild, non-eruptive seepage (i.e. the extinct MV, the coral ridges and the CWC
369 Mound Fields: **Figs. 3 and 6**). The observation that these systems are in large parts “coral graveyards” (**Fig. 6, B–**
370 **D**), similar to other areas in the Gulf of Cádiz (see Foubert et al., 2008; Wienberg et al., 2009), may be explained
371 by a post-glacial decrease in current strength (Foubert et al., 2008). In the light of our findings, however, they
372 could also have been negatively affected by periods of intensive seepage during higher tectonic activity. Future
373 studies are important to test this hypothesis in greater detail.

374 **4.3. Spatio-temporal co-existence of CWCs and chemosynthetic organisms — the buffer effect**

375 As discussed above, MDAC deposits are ecologically beneficial for CWCs, as they served as optimal substrata
376 even when seepage is still present (e. g. Hovland, 1990; Hovland & Thomsen, 1997; Le Guilloux et al., 2009; this
377 study). Severe hydrocarbon-rich seepage, however, is ecologically stressful for the corals. Particularly, fluid- and
378 AOM-derived hydrogen sulfide is considered problematic because of its role in coral necrosis (Myers &
379 Richardson, 2009; García et al., 2016) and carbonate dissolution effects (Wehrmann et al., 2011).

380 Hydrogen sulfides can efficiently be buffered through the reaction with Fe-(oxyhydro)-oxides or Fe^{2+} dissolved in
381 pore waters, ultimately forming pyrite (Wehrmann et al., 2011). Fe-(oxyhydro)-oxides nodules have previously
382 been observed in the Iberian and Moroccan margins (González et al., 2009; 2012b), but not in the Pompeia
383 Province. Instead, sulfide-oxidizing bacteria living in symbiosis with invertebrates (e.g. siboglinid worms:



384 Petersen & Dubilier, 2009) (**Fig. 5, D**) and thriving in mats (**Fig. 4, C**; **Fig. 6, A**) were particularly prominent along
385 this region. Furthermore, the consumption of methane and sulfate by AOM-microorganisms at active sites also
386 contribute to CWCs colonization of the carbonates by reducing environmental acidification.

387 An integrated model is proposed to represent the biological buffer effect observed in different cases along the
388 Pompeia Province. On the one hand, pockmark sites at the Al Gacel MV display the co-existence of non-
389 chemosynthetic corals (e.g. on top of D10-R7 carbonate; **Fig. 5**) with AOM-microorganisms and chemosynthetic
390 sulfide-oxidizing organisms (**Fig. 12, A**). Likewise, diapiric ridges (**Fig. 12, B**) and coral mounds (**Fig. 12, C**) may
391 similarly prevent CWCs dissolution, as observed in the Northern Pompeia Coral Ridge, where sulfide-oxidizing
392 bacterial mats were tightly related to the scleractinian-coral carbonates colonized by other non-chemosynthetic
393 octocorals (**Fig. 6**). This model represents the first approach on understanding the ecological linkage between
394 hydrocarbon-rich seepage and cold-water corals. The impact and exact capacity of this biological buffer, however,
395 remains elusive and must be evaluated in future studies.

396 **5. Conclusions**

397 The presence of cold-water corals related to hydrocarbon-seep structures like mud volcanoes and diapirs, is partly
398 due to the irregular topography affecting bottom water-currents, which supply nutrients to the corals. Likewise,
399 their tight-linkage to active hydrocarbon-rich seepage occurs by means of the production of methane-derived
400 carbonates and how they provide the hard substrata cold-water corals need to develop. The discovery of methane-
401 derived carbonates with embedded corals evidences the decline of coral colonization when the intensity of the
402 fluid seepage increases or becomes more violent. Consequently, cold-water coral growth in these habitats depends
403 directly on seepage intensity and how these fluids are drained onto the seafloor (i.e. eruptive, focused, diffused or
404 dripping-like). Furthermore, cold-water corals rely on the microbial AOM-metabolism and sulfide oxidation to
405 reduce seeped fluids in the environment, since they are harmful for the corals. This biological buffer is possibly
406 crucial to keep conditions favorable for the growth of cold-water corals in the studied area, particularly in times
407 of increased fluid seepage.

408 **Author contribution**

409 Blanca Rincón-Tomás, Dominik Schneider and Michael Hoppert carried out the microbial analysis. Jan-Peter
410 Duda carried out the biomarker analysis. Luis Somoza and Teresa Medialdea processed seismic and bathymetric
411 data. Pedro Madureira processed ROV data. Javier González and Joachim Reitner carried out the petrographic
412 analysis. Joachim Reitner carried out the stable isotopic analysis. Blanca Rincón-Tomás prepared the manuscript
413 with contributions from all co-authors.

414 **Competing interests**

415 The authors declare that they have no conflict of interest.

416 **Acknowledgments**

417 The authors thank the captain and the crew on board the R/V Sarmiento de Gamboa, as well as the UTM (Unidad
418 de Tecnología Marina), that have been essential for the success of this paper. Data obtained on board is collected



419 in the SUBVENT-2 cruise, which can be found in the IGME archive. This work was supported by the Spanish
420 project SUBVENT (CGL2012-39524-C02) and the project EXPLOSEA (CTM2016-75947) funded by the Spanish
421 Ministry of Science, Innovation and Universities.

422 References

- 423 Ahmed, M. and George, S.C.: Changes in the molecular composition of crude oils during their preparation for GC
424 and GC–MS analyses, *Org. Geochem.*, 35, 137–155, doi:10.1016/j.orggeochem.2003.10.002, 2004.
- 425 Becker, E. L., Cordes, E. E., Macko, S. A., and Fisher, C. R.: Importance of seep primary production to *Lophelia*
426 *pertusa* and associated fauna in the Gulf of Mexico, *Deep-sea Res Pt I*, 56(5), 786–800,
427 doi:10.1016/j.dsr.2008.12.006, 2009.
- 428 Birgel, D., Thiel, V., Hinrichs, K. U., Elvert, M., Campbell, K. A., Reitner, J., Farmer, J. D., and Peckmann, J.:
429 Lipid biomarker patterns of methane-seep microbialites from the Mesozoic convergent margin of
430 California, *Org. Geochem.*, 37(10), 1289–1302, doi:10.1016/j.orggeochem.2006.02.004, 2006.
- 431 Boetius, A., Ravenschlag, K., Schubert, C. J., Rickert, D., Widdel, F., Gieseke, A., Amann, R., Jørgensen, B. B.,
432 Witte, U., and Pfannkuche, O.: A marine microbial consortium apparently mediating anaerobic oxidation
433 of methane, *Nature*, 407 (6804), 623–626, doi:10.1038/35036572, 2000.
- 434 Boetius, A., and Suess, E.: Hydrate Ridge: a natural laboratory for the study of microbial life fueled by methane
435 from near-surface gas hydrates, *Chem. Geol.*, 205, 291–310, doi:10.1016/j.chemgeo.2003.12.034, 2004.
- 436 Callahan, B., MacMurdie, P. J., and Holmes, S. O.: Exact sequence variants should replace optional taxonomic
437 units in marker-gene data analysis, *ISME J.*, 11, 2639–2643, doi:10.1038/ismej.2017.119, 2017.
- 438 Caporaso, J.G., Kuczynski, J., Stombaugh, J., Bittinger, K., Bushman, F.D., Costello, E.K., Fierer, N., González-
439 Peña, A., Goodrich, J. K., Gordon, J. I., Huttley, G. A., Knights, D., Koenig, J. E., Lozupone, C. A.,
440 McDonald, D., Muegge, B. D., Pirrung, M., Reeder, J., Sevinsky, J. R., Turnbaugh, P. J., Walters, W. A.,
441 Widmann, J., Yatsunenko, T., Zaneveld, J., and Knight, R.: QIIME allows analysis of high-throughput
442 community sequencing data, *Nat. Methods*, 7, 335–336, doi:10.1038/nmeth.f.303, 2010.
- 443 Cordes, E., Arnaud-Haond, S., Bergstad, O., da Costa Falcão, A. P., Freiwald, A., Roberts, J. M., and Bernal, P.:
444 Cold water corals, in: *The First Global Integrated Marine Assessment, World Ocean Assessment I*, United
445 Nations, Cambridge University Press, Cambridge, United Kingdom, 2016.
- 446 Díaz-del-Río, V., Somoza, L., Martínez-Frías, J., Mata, M. P., Delgado, A., Hernandez-Molina, F. J., ..., Vázquez,
447 J. T.: Vast fields of hydrocarbon-derived carbonate chimneys related to the accretionary
448 wedge/olistostrome of the Gulf of Cádiz, *Mar. Geol.*, 195, 177–200, doi:10.1016/S0025-3227(02)00687-
449 4, 2003.
- 450 Dorschel, B., Hebbeln, D., Foubert, A., White, M., and Wheeler, A. J.: Hydrodynamics and cold-water coral facies
451 distribution related to recent sedimentary processes at Galway Mound west of Ireland, *Mar. Geol.*, 244,
452 184–195, doi:10.1016/j.margeo.2007.06.010, 2007.
- 453 Duineveld, G. C., Lavaleye, M. S., Bergman, M. J., De Stigter, H., and Mienis, F.: Trophic structure of a cold-
454 water coral mound community (Rockall Bank, NE Atlantic) in relation to the near-bottom particle supply
455 and current regime, *B. Mar. Sci.*, 81 (3), 449–467, 2007.



- 456 Dullo, W. C., Flögel, S., and Rüggerberg, A.: Cold-water coral growth in relation to the hydrography of the Celtic
457 and Nordic European continental margin, *Mar. Ecol. Prog. Ser.*, 371, 165–176, doi:10.3354/meps07623,
458 2008.
- 459 Dunham, R. J., 1962, Classification of carbonate rocks according to their depositional texture, in: Classification
460 of Carbonate Rocks, Ham, W. E. (Eds.), American Association of Petroleum Geologists Memoir 1, Tulsa,
461 OK, 108–121, 1962.
- 462 Edgar, R. C.: USEARCH. <http://www.drive5.com/usearch>. 2010.
- 463 Egelkamp, R., Schneider, D., Hertel, R., and, Daniel, R.: Nitrile-Degrading Bacteria Isolated from Compost, *Front.*
464 *Environ. Sci.*, 5, doi: 10.3389/fenvs.2017.00056, 2017.
- 465 Embry III, A. F., and Klovan, J. E.: A late Devonian reef tract on northeastern Banks Island, NWT, *B. Can. Petrol.*
466 *Geol.*, 19(4), 730–781, 1971.
- 467 Foubert, A., Depreiter, D., Beck, T., Maignien, L., Pannemans, B., Frank, N., Blamart, D., and Henriët, J.:
468 Carbonate mounds in a mud volcano province off north-west Morocco: key to processes and controls,
469 *Mar. Geol.*, 248, 74–96, doi: 10.1016/j.margeo.2007.10.012, 2008.
- 470 Frank, N., Freiwald, A., López-Correa, M., Wienberg, C., Eisele, M., Hebbeln, D., Van Rooj, D., Henriët, J.-P.,
471 Colin, C., van Weering, T., de Haas, H., Buhl-Mortensen, P., Roberts, J. M., De Mol, B., Douville, E.,
472 Blamart, D., and Hatté, C.: Northeastern Atlantic cold-water coral reefs and climate, *Geology*, 39 (8),
473 743–746, doi:10.1130/G31825.1, 2011.
- 474 Freiwald, A., Hühnerbach, V., Lindberg, B., Wilson, J., and Campbell, J.: The Sula Reef Complex, Norwegian
475 Shelf, *Facies*, 47, 179–200, doi:10.1007/BF02667712, 2002.
- 476 Freiwald, A., Wilson, J. B., and Henrich, R.: Grounding Pleistocene icebergs shape recent deep water coral reefs,
477 *Sedimentary Geology* 125, 1–8, doi:10.1016/S0037-0738(98)00142-0, 1999.
- 478 Garcia, G. D., Santos, E. D. O., Sousa, G. V., Zingali, R. B., Thompson, C. C., and Thompson, F. L.:
479 Metaproteomics reveals metabolic transitions between healthy and diseased stony coral *Mussismilia*
480 *braziliensis*, *Mol. Ecol.*, 25(18), 4632–4644, doi:10.1111/mec.13775, 2016.
- 481 Gomes-Sumida, P.Y., Yoshinaga, M.Y., Saint-Pastous Madureira, L.A., and Hovland, M.: Seabed pockmarks
482 associated with deep water corals off SE Brazilian continental slope, Santos Basin, *Mar. Geol.*, 207, 159–
483 167, doi:10.1016/j.margeo.2004.03.006, 2004.
- 484 González, F. J., Somoza, L., Lunar, R., Martínez-Frías, J., Martín Rubí, J. A., Torres, T., Ortiz, J. E., Díaz-del-
485 Río, V., Pinheiro, L. M., and Magalhães, V. H.: Hydrocarbon-derived ferromanganese nodules in
486 carbonate mud mounds from the Gulf of Cádiz: mud-breccia sediments and clasts as nucleation sites,
487 *Mar. Geol.*, 261, 64–81, doi:10.1016/j.margeo.2008.11.005, 2009.
- 488 González, F. J., Somoza, L., León, R., Medialdea, T., de Torres, T., Ortiz, J. E., Martínez-Frías, J., and Merinero,
489 R.: Ferromanganese nodules and micro-hardgrounds associated with the Cádiz Contourite Channel (NE
490 Atlantic): Palaeoenvironmental records of fluid venting and bottom currents, *Chem. Geol.*, 310–311, 56–
491 78, doi: 10.1016/j.chemgeo.2012.03.030, 2012a.
- 492 González, F. J., Somoza, L., Medialdea, T., León, R., Torres, T., Ortiz, J. E., and Martín-Rubí, J. A.: Discovery of
493 ferromanganese hydrocarbon-related nodules associated with the Meknes mud volcano (Western
494 Moroccan margin). European Geoscience Union 2012 (EGU2012). Viena (Austria). *Geophys. Res. Abs.*
495 vol. 14, EGU2012-12306, 2012b.



- 496 Hebbeln, D., Van Rooij, D., and Wienberg, C.: Good neighbours shaped by vigorous currents: cold-water coral
497 mounds and contourites in the North Atlantic, *Mar. Geol.*, 378, 171–185,
498 doi:10.1016/j.margeo.2016.01.014, 2016.
- 499 Hensen, C., Nuzzo, M., Hornibrook, E., Pinheiro, L.M., Bock, B., Magalhães, V.H., and Brückmann, W.: Sources
500 of mud volcano fluids in the Gulf of Cádiz — indications for hydrothermal imprint, *Geochim.*
501 *Cosmochim. Ac.*, 71 (5), 1232–1248, doi:10.1016/j.gca.2006.11.022, 2007.
- 502 Hinrichs, K. -U., and Boetius, A.: The anaerobic oxidation of methane: new insights in microbial ecology and
503 biogeochemistry, in: *Ocean Margin Systems*, Wefer, G., Billett, D., Hebbeln, D., Jørgensen, B.B.,
504 Schlueter, M., Van Weering, T. (Eds.), Springer-Verlag, Berlin, 457–477, 2002.
- 505 Hinrichs, K. -U., Hayes, J. M., Sylva, S. P., Brewer, P. G., and De Long, E. F.: Methane-consuming archaeobacteria
506 in marine sediments, *Nature*, 398, 802–805, doi:10.1038/19751, 1999.
- 507 Hoefs, J.: *Stable Isotope Geochemistry*, Springer, Berlin, 2015.
- 508 Hovland, M.: Do carbonate reefs form due to fluid seepage?, *Terra Nova*, 2, 8–18, doi:10.1111/j.1365-
509 3121.1990.tb00031.x, 1990.
- 510 Hovland, M., Jensen, S., and Indreien, T.: Unit pockmarks associated with *Lophelia* coral reefs off mid-Norway:
511 more evidence of control by ‘fertilizing’ bottom currents, *Geo-Mar. Lett.*, 32 (5–6), 545–554,
512 doi:10.1007/s00367-012-0284-0, 2012.
- 513 Hovland, M., Mortensen, P. B., Brattegard, T., Strass, P., and Rokoengen, K.: Ahermatypic coral banks off mid-
514 Norway: evidence for a link with seepage of light hydrocarbons, *Palaios*, 13, 189–200, doi:10.1043/0883-
515 1351(1998)013<0189:ACBOME>2.0.CO;2, 1998.
- 516 Hovland, M., and Thomsen, E.: Cold-water corals — are they hydrocarbon seep related?, *Mar. Geol.*, 137, 159–
517 164, doi:10.1016/S0025-3227(96)00086-2, 1997.
- 518 Huvenne, V. A., Masson, D. G., and Wheeler, A. J.: Sediment dynamics of a sandy contourite: the sedimentary
519 context of the Darwin cold-water coral mounds, Northern Rockall Trough, *Int. J. Earth Sci.*, 98 (4), 865–
520 884, doi: 10.1007/s00531-008-0312-5, 2009.
- 521 Ivanov, M. K., Akhmetzhanov, A. M., and Akhmanov, G. G.: Multidisciplinary study of geological processes on
522 the North East Atlantic and Western Mediterranean Margins, in: *Ioc. Tech. S.*, 56, UNESCO, 2000.
- 523 Kiriakoulakis, K., Fisher, E., Wolff, G. A., Freiwald, A., Grehan, A., and Roberts, J. M.: Lipids and nitrogen
524 isotopes of two deep-water corals from the North-East Atlantic: initial results and implications for their
525 nutrition, in: *Cold-Water Corals and Ecosystems*, Freiwald, A., Roberts, J. M. (Eds.), Erlangen Earth
526 Conf., Springer, Germany, 715–729, 2005.
- 527 Le Bris, N., Arnaud-Haond, S., Beaulieu, S., Cordes, E. E., Hilario, A., Rogers, A., van de Gaever, S., and
528 Watanabe, H.: Hydrothermal Vents and Cold Seeps, in: *The First Global Integrated Marine Assessment*,
529 United Nations, Cambridge University Press, Cambridge, United Kingdom, 2016.
- 530 Le Guilloux, E., Olu, K., Bourillet, J. F., Savoye, B., Iglésias, S. P., and Sibuet, M.: First observations of deep-sea
531 coral reefs along the Angola margin, *Deep-sea Res. Pt. II*, 56, 2394–2403,
532 doi:10.1016/j.dsr2.2009.04.014, 2009.
- 533 Liebetrau, V., Eisenhauer, A., and Linke, P.: Cold seep carbonates and associated cold-water corals at the
534 Hikurangi Margin, New Zealand: new insights into fluid pathways, growth structures and geochronology,
535 *Mar. Geol.*, 272, 307–318, doi:10.1016/j.margeo.2010.01.003, 2010.



- 536 León, R., Somoza, L., Medialdea, T., Vázquez, J. T., González, F. J., López-González, N., Casas, D., del Pilar
537 Mata, M., del Fernández-Puga, C., Giménez-Moreno, C. J., and Díaz-del-Río, V.: New discoveries of
538 mud volcanoes on the Moroccan Atlantic continental margin (Gulf of Cádiz): morpho-structural
539 characterization, *Geo-Mar. Lett.*, 32, 473–488, doi:10.1007/s00367-012-0275-1, 2012.
- 540 Magalhães, V. H., Pinheiro, L. M., Ivanov, M. K., Kozlova, E., Blinova, V., Kolganova, J., Vasconcelos, C.,
541 McKenzie, J. A., Bernasconi, S. M., Kopf, A., Díaz-del-Río, V., González, F. J., and Somoza, L.:
542 Formation processes of methane-derived authigenic carbonates from the Gulf of Cádiz, *Sediment. Geol.*,
543 243–244, 155–168, doi:10.1016/j.sedgeo.2011.10.013, 2012.
- 544 Margreth, S., Gennari, G., Rüggeberg, A., Comas, M. C., Pinheiro, L. M., and Spezzferri, S.: Growth and demise
545 of cold-water coral ecosystems on mud volcanoes in the West Alboran Sea: The messages from planktonic
546 and benthic foraminifera, *Mar. Geol.*, 282, 26–39, doi:10.1016/j.margeo.2011.02.006, 2011.
- 547 Martin, M.: Cutadapt removes Adapter Sequences from High-Throughput Sequencing Reads, *EMBnet.journal*, 10–
548 12, doi: 10.14806/ej.17.1.200, 2011.
- 549 Medialdea, T., Somoza, L., Pinheiro, L. M., Fernández-Puga, M. C., Vázquez, J. T., León, R., Ivanov, M. K.,
550 Magalhães, V., Díaz-del-Río, V., and Vegas, R.: Tectonics and mud volcano development in the Gulf of
551 Cádiz, *Mar. Geol.*, 261, 48–63, doi:10.1016/j.margeo.2008.10.007, 2009.
- 552 Mortensen, P. B., Hovland, M. T., Fossa, J. H., and Furevik, D. M.: Distribution, abundance and size of *Lophelia*
553 *pertusa* coral reefs in mid Norway in relation to seabed characteristics, *J. Mar. Biol. Assoc. UK*, 81, 581–
554 597, doi:10.1017/S002531540100426X, 2001.
- 555 Myers, J.L., and Richardson, L.L.: Adaptation of cyanobacteria to the sulfide-rich microenvironment of black band
556 disease of coral, *FEMS Microbiol. Ecol.*, 67, 242–251, doi:10.1111/j.1574-6941.2008.00619.x, 2009.
- 557 Peckmann, J., Reimer, A., Luth, U., Luth, C., Hansen, B.T., Heinicke, C., Hoefs, J., and Reitner, J.: Methane-
558 derived carbonates and authigenic pyrite from the northwestern Black Sea, *Mar. Geol.*, 177, 129–150,
559 doi:10.1016/S0025-3227(01)00128-1, 2001.
- 560 Peckmann, J., and Thiel, V.: Carbon cycling at ancient methane-seeps, *Chem. Geol.*, 205 (3), 443–467,
561 doi:10.1016/j.chemgeo.2003.12.025, 2004.
- 562 Petersen, J. M., and Dubilier, N.: Methanotrophic symbioses in marine invertebrates, *Env. Microbiol. Rep.*, 1(5),
563 319–335, doi:10.1111/j.1758-2229.2009.00081.x, 2009.
- 564 Pinheiro, L. M., Ivanov, M. K., Sautkin, A., Akhmanov, G., Magalhães, V. H., Volkonskaya, A., Monteiro, J. H.,
565 Somoza, L., Gardner, J., Hamouni, N., and Cunha, M. R.: Mud volcanism in the Gulf of Cádiz: results
566 from the TTR-10 cruise, *Mar. Geol.*, 195, 131–151, doi:10.1016/S0025-3227(02)00685-0, 2003.
- 567 Rådecker, N., Pogoreutz, C., Voolstra, C. R., Wiedenmann, J., and Wild, C.: Nitrogen cycling in corals: The key
568 to understanding holobiont functioning?, *Trends Microbiol.*, 23 (8), 490–497,
569 doi:10.1016/j.tim.2015.03.008, 2015.
- 570 Reitner, J., Gauret, P., Marin, F., and Neuweiler, F.: Automicrites in a modern marine microbialite. Formation
571 model via organic martices (Lizard Island, Great Barrier Reef, Australia), *Bull.-Inst. Oceanogr. Monaco*,
572 14, 237–263, 1995.
- 573 Reitner, J., Peckmann, J., Blumenberg, M., Michaelis, W., Reimer, A., and Thiel, V.: Concretionary methane-seep
574 carbonates and associated microbial communities in Black Sea sediments, *Palaeogeogr., Palaeoclimatol.,*
575 *Palaeocl.*, 227, 18–30, doi:10.1016/j.palaeo.2005.04.033, 2005.



- 576 Roberts, J. M., Long, D., Wilson, J. B., Mortensen, P. B., and Gage, J. D.: The cold-water coral *Lophelia pertusa*
577 (Scleractinia) and enigmatic seabed mounds along the north-east Atlantic margin: are they related?, Mar.
578 Pollut. Bull., 46, 7–20, doi:10.1016/S0025-326X(02)00259-X, 2003.
- 579 Roberts, J. M., Wheeler, A. J., and Freiwald, A.: Reefs of the deep: the biology and geology of cold-water coral
580 ecosystems, Science, 312 (5773), 543–547, doi:10.1126/science.1119861, 2006.
- 581 Roberts, J. M., Wheeler, A., Freiwald, A., and Cairns, S. (Eds.): Cold-water corals: the biology and geology of
582 deep-sea coral habitats, Cambridge University Press, Cambridge, United Kingdom, 2009.
- 583 Rodrigues, C. F., Cunha, M. R., Génio, L., and Duperron, S.: A complex picture of associations between two host
584 mussels and symbiotic bacteria in the Northeast Atlantic, Naturwissenschaften, 100, 21–31,
585 doi:10.1007/s00114-012-0985-2, 2013.
- 586 Rogers, A. D.: The Biology of *Lophelia pertusa* (Linnaeus 1758) and other Deep-Water Reef-Forming Corals and
587 Impacts from Human Activities, Int. Rev. Hydrobiol., 84 (4), 315–406, doi:10.1002/iroh.199900032,
588 1999.
- 589 Rueda, J. L., González-García, E., Krutzky, C., López-Rodríguez, J., Bruque, G., López-González, N., Palomino,
590 D., Sánchez, R. F., Vázquez, J. T., Fernández-Salas, L. M., and Díaz-del-Río, V.: From chemosynthetic-
591 based communities to cold-water corals: Vulnerable deep-sea habitats of the Gulf of Cádiz, Mar.
592 Biodiver., 46, 473–482, doi:10.1007/s12526-015-0366-0, 2016.
- 593 Sánchez-Guillamón, O., García, M. C., Moya-Ruiz, F., Vázquez, J. T., Palomino, D., Fernández-Puga, M. C., and
594 Sierra, A.: A preliminary characterization of greenhouse gas (CH₄ and CO₂) emissions from Gulf of Cádiz
595 mud volcanoes, VIII Symposium MIA15, 2015.
- 596 Scholz, F., Hensen, C., Reitz, A., Romer, R. L., Liebetrau, V., Meixner, A., Weise, S. M., and Haeckel, M.: Isotopic
597 evidence (⁸⁷Sr/⁸⁶Sr, ^δ7Li) for alteration of the oceanic crust at deep-rooted mud volcanoes in the Gulf
598 of Cádiz, NE Atlantic Ocean, Geochim. Cosmochim. Ac., 73, 5444–5459, doi:10.1016/j.gca.2009.06.004,
599 2009.
- 600 Smith, P., Reay, D., and Van Amstel, A. (Eds.): Methane and climate change, Earthscan, London, Washington
601 D.C., 2010.
- 602 Somoza, L., Ercilla, G., Urgorri, V., León, R., Medialdea, T., Paredes, M., González, F. J., and Nombela, M. A.:
603 Detection and mapping of cold-water coral mounds and living *Lophelia* reefs in the Galicia Bank, Atlantic
604 NW Iberia margin, Mar. Geol., 349, 73–90, doi:10.1016/j.margeo.2013.12.017, 2014.
- 605 Somoza, L., León, R., Ivanov, M., Fernández-Puga, M. C., Gardner, J. M., Hernández-Molina, F. J., Pinheiro, L.
606 M., Rodero, J., Lobato, A., Maestro, A., Vázquez, J. T., Medialdea, T., and Fernández-Salas, L. M.:
607 Seabed morphology and hydrocarbon seepage in the Gulf of Cádiz mud volcano area: Acoustic imagery,
608 multibeam and ultra-high resolution seismic data, Mar. Geol., 195, 153–176, doi:10.1016/S0025-
609 3227(02)00686-2, 2003.
- 610 Sorokin, Y. I.: Coral reef ecology, Springer, Germany, 1995.
- 611 Suess, E. and Whiticar, M. J.: Methane-derived CO₂ in pore fluids expelled from the Oregon subduction zone,
612 Palaeogeogr., Palaeoclimatol., Palaeocl., 71, 119–136, doi:10.1016/0031-0182(89)90033-3, 1989.
- 613 Thiel, V., Peckmann, J., Seifert, R., Wehrung, P., Reitner, J., and Michaelis, W.: Highly isotopically depleted
614 isoprenoids: molecular markers for ancient methane venting, Geochim. Cosmochim. Ac., 63, 3959–3966,
615 doi:10.1016/S0016-7037(99)00177-5, 1999.



- 616 Thiel, V., Peckmann, J., Richnow, H.-H., Luth, U., Reitner, J., and Michaelis, W.: Molecular signals for anaerobic
617 methane oxidation in Black Sea seep carbonates and a microbial mat, *Mar. Chem.* 73, 97–112,
618 doi:10.1016/S0304-4203(00)00099-2, 2001.
- 619 Thiem, Ø., Ravagnan, E., Fosså, J. H., and Berntsen, J.: Food supply mechanisms for cold- water corals along a
620 continental shelf edge, *J. Marine Syst.*, 26, 1481–1495, doi:10.1016/j.jmarsys.2005.12.004, 2006.
- 621 Valentine, D. L.: Biogeochemistry and microbial ecology of methane oxidation in anoxic environments: a review,
622 A. Van Leeuw. *J. Microb.*, 81, 271–282, doi:10.1023/A:1020587206351, 2002.
- 623 Vandorpe, T., Martins, I., Vitorino, J., Hebbeln, D., García-García, M., and Van Rooij, D.: Bottom currents and
624 their influence on the sedimentation pattern in the El Arraiche mud volcano province, southern Gulf of
625 Cádiz, *Mar. Geol.*, 378, 114–126, doi:10.1016/j.margeo.2015.11.012, 2016.
- 626 Vandorpe, T., Wienberg, C., Hebbeln, D., Van den Berghe, M., Gaide, S., Wintersteller, P., and Van Rooij, D.:
627 Multiple generations of buried cold-water coral mounds since the Early-Middle Pleistocene Transition in
628 the Atlantic Moroccan Coral Province, southern Gulf of Cádiz, *Palaeogeogr., Palaeoclimatol., Palaeocl.*,
629 485, 293–304, doi:10.1016/j.palaeo.2017.06.021, 2017.
- 630 Van Rensbergen, P., Depreiter, D., Pannemans, B., Moerkerke, G., Van Rooij, D., Marsset, B., Akhmanov, G.,
631 Blinova, V., Ivanov, M., Rachidi, M., Magalhães, V., Pinheiro, L., Cunha, M., and Henriët, J.P.: The
632 Arraiche mud volcano field at the Moroccan Atlantic slope, Gulf of Cádiz, *Mar. Geol.*, 219, 1–17,
633 doi:10.1016/j.margeo.2005.04.007, 2005.
- 634 Van Rooij, D., Blamart, D., De Mol, L., Mienis, F., Pirllet, H., Whermann, L. M., ..., Henriët, J. -P.: Cold-water
635 coral mounds on the Pen Duick Escarpment, Gulf of Cádiz: The MiCROSYSTEMS project approach,
636 *Mar. Geol.*, 282, 102–117, doi:10.1016/j.margeo.2010.08.012, 2011.
- 637 Watling, L., France, S. C., Pante, E., and Simpson, A.: Biology of Deep-Water Octocorals, in: *Advances in Marine*
638 *Biology Volume 60*, Lesser, M. (Eds.), Academic Press, London, United Kingdom, 41–122, 2011.
- 639 Webster, N. S., Negri, A. P., Botté, E. S., Laffy, P. W., Flores, F., Noonan, S., Schmidt, C., and Uthicke, S.: Host-
640 associated coral reef microbes respond to the cumulative pressures of ocean warming and ocean
641 acidification *Sci. Rep.-UK*, 6, doi:10.1038/srep19324, 2016.
- 642 Wheeler, A. J., Beyer, A., Freiwald, A., de Haas, H., Huvenne, V. A., Kozachenko, M., Olu-Le Roy, K.,
643 and Opderbecke, J.: Morphology and environment of cold-water coral carbonate mounds on the NW
644 European margin, *Int. J. Earth Sci.*, 96, 37–56, doi:10.1007/s00531-006-0130-6, 2007.
- 645 Wehrmann, L. M. Templer, S. P., Brunner, B., Bernasconi, S. M., Maignien, L., and Ferdelman, T. G.: The imprint
646 of methane seepage on the geochemical record an early diagenetic processes in cold-water coral mounds
647 on Pen Duick Escarpment, Gulf of Cádiz, *Mar. Geol.*, 118–137, doi:10.1016/j.margeo.2010.08.005, 2011.
- 648 Wienberg, C., Hebbeln, D., Fink, H. G., Mienis, F., Dorschel, B., Vertino, A., López-Correa, M., and Freiwald,
649 A.: Scleractinian cold-water corals in the Gulf of Cádiz—first clues about their spatial and temporal
650 distribution, *Deep-sea Res. Pt. I*, 56 (10), 1873–1893, doi:10.1016/j.dsr.2009.05.016, 2009.
- 651 Wienberg, C., and Titschack, J.: Framework-forming scleractinian cold-water corals through space and time: a
652 late Quaternary North Atlantic perspective, in: *Marine Animal Forests: The Ecology of Benthic*
653 *Biodiversity Hotspots*, Rossi, S., Bramanti, L., Gori, A., and Orejas, C. (Eds.), Springer, Cham,
654 Switzerland, 1–34, 2015.



655 Yilmaz, P., Parfrey, L.W., Yarza, P., Gerken, J., Pruese, E., Quast, C., Schweer, T., Peplies, J., Ludwig, W., and
656 Glöckner, F. O.: The SILVA and ‘All-species Living Tree Project (LTP)’ taxonomic frameworks, *Nucleic*
657 *Acids Res.*, 42, D643–D648, doi:10.1093/nar/gkt1209, 2014.

658 Zhang, J., Kobert, K., Flouri, T., and Stamatakis, A.: PEAR: a fast and accurate Illumina Paired-End reAd
659 merger, *Bioinformatics*, 30 (5), 614–620, doi:10.1093/bioinformatics/btt593, 2014.

660

661

662

663

664

665

666

667

668

669

670

671

672

673

674

675

676

677

678

679

680

681

682

683

684

685

686

687

688

689

690

691

692

693

694

695



696 **Table 1.** *In-situ* water variables measured during sampling with ROV sensors.

	D10-R3	D10-R7	D11-R8	D03-B1
Temperature (°C)	10.07	10.5	10.02	10.04 – 10.05
Depth (m)	850 – 890	791	763	829
Conductivity (mS/cm)	39.13 – 39.62	39.05 – 39.43	-	-
Salinity (ppt)	-	-	35.56 – 35.86	35.67 – 35.91
Saturation of dissolved oxygen (%)	53.64 – 54.69	54.02 – 54.35	51.95 – 53.92	52.46 – 56.22
Dissolved oxygen (mg/l)	4.81 – 4.90	4.85 – 4.88	4.66 – 4.84	4.71 – 5.09
Density (kg/m ³)	31.03 – 31.42	30.94 – 31.24	30.92 – 31.08	31.26 – 31.41

697

698

699

700

701

702

703

704

705

706

707

708

709

710

711

712

713

714

715

716

717

718

719

720

721



722 **Table 2.** Stable carbon and oxygen isotopes ($\delta^{13}\text{C}$, $\delta^{18}\text{O}$) of samples from the Al Gacel MV and the Northern
 723 Pompeia Coral Ridge.

Location	Sample	Identifier	$\delta^{18}\text{O}$ (‰)	$\delta^{13}\text{C}$ (‰)
Al Gacel MV	D10-R3	1	2.35	-5.58
		2	3.37	-20.07
		3	3.60	-26.68
		4	3.70	-20.79
		5	3.45	-22.43
		6	3.80	-20.70
		7	3.28	-2.23
		8	3.83	-25.16
		9	3.63	-25.29
		10	3.91	-18.38
		11	3.60	-24.18
		12	3.55	-25.34
		13	3.56	-25.15
		14	3.50	-2.09
		15	3.92	-21.89
Al Gacel MV	D10-R7	21	2.90	-26.36
		22	3.15	-28.77
		23	2.94	-22.91
		24	2.67	-21.13
		25	2.37	-24.70
		26	2.56	-23.60
Al Gacel MV	D11-R8	16	1.49	-4.91
		17	2.13	-2.99
		18	1.74	-4.22
		19	5.60	-14.82
		20	5.55	-14.74
Coral Ridge	D03-B1	1.1	-0.38	-7.93
		1.2	-0.86	-7.77
		1.3	-0.51	-7.35
		1.5	1.15	-5.26
		1.4	-1.03	-8.08
		1.6	0.69	-5.96
		1.7	0.54	-6.42

724

725

726 **Table 2.** Continued

Location	Sample	Identifier	$\delta^{18}\text{O}$ (‰)	$\delta^{13}\text{C}$ (‰)
Coral Ridge	D03-B1	3.1	1.59	-2.08
		3.2	-0.31	-6.27
		3.3	-0.89	-6.78
		3.4	-0.94	-6.73
		3.5	1.84	-2.21
		3.6	2.26	-1.39
		3.7	1.74	-2.87

727

728

729 **Table 3.** Stable carbon isotopic composition ($\delta^{13}\text{C}$) of selected lipid biomarkers (in **Figure 10**). (*) Please note

730 that crocetane in D11-R8 coelutes with phytane. n.d. = not detected.

Compound	D10-R7 (‰)	D11-R8 (‰)
<i>n</i> -C ₁₇	n.d.	-33.0
<i>n</i> -C ₁₈	n.d.	-31.8
<i>n</i> -C ₁₉	n.d.	-31.1
<i>n</i> -C ₂₀	n.d.	-30.8
<i>n</i> -C ₂₁	n.d.	-31.5
<i>n</i> -C ₂₂	n.d.	-31.7
Crocetane*	-101.2	-57.2
PMI	-102.9	-74.3

731

732

733

734

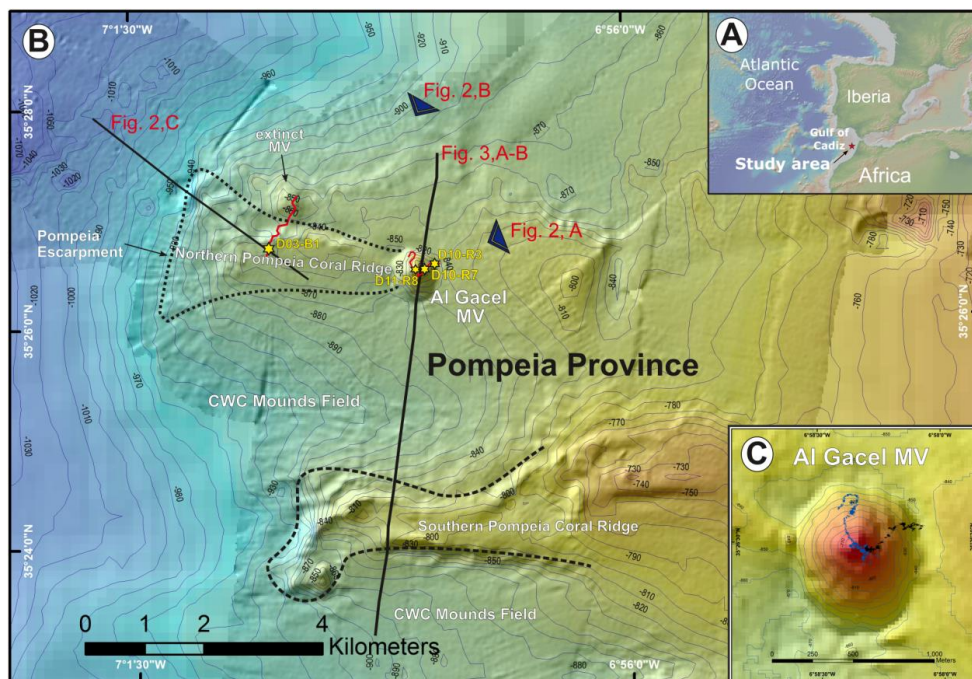
735

736

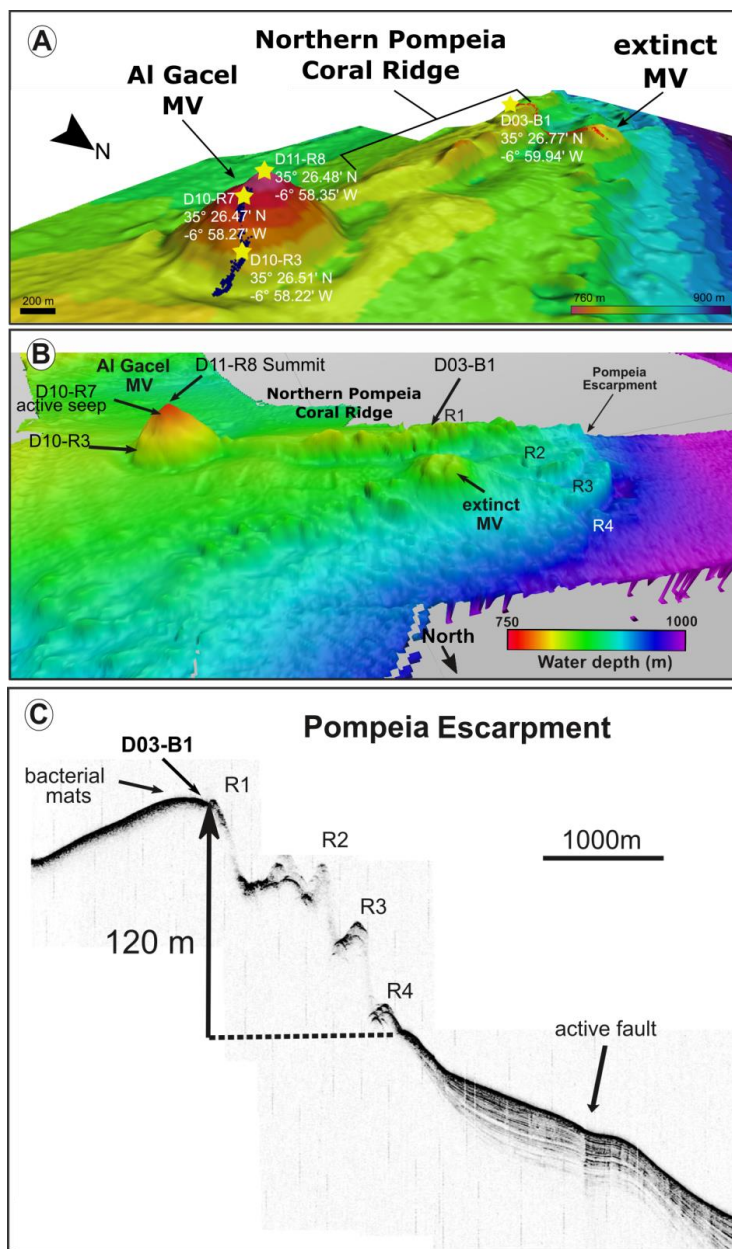
737

738

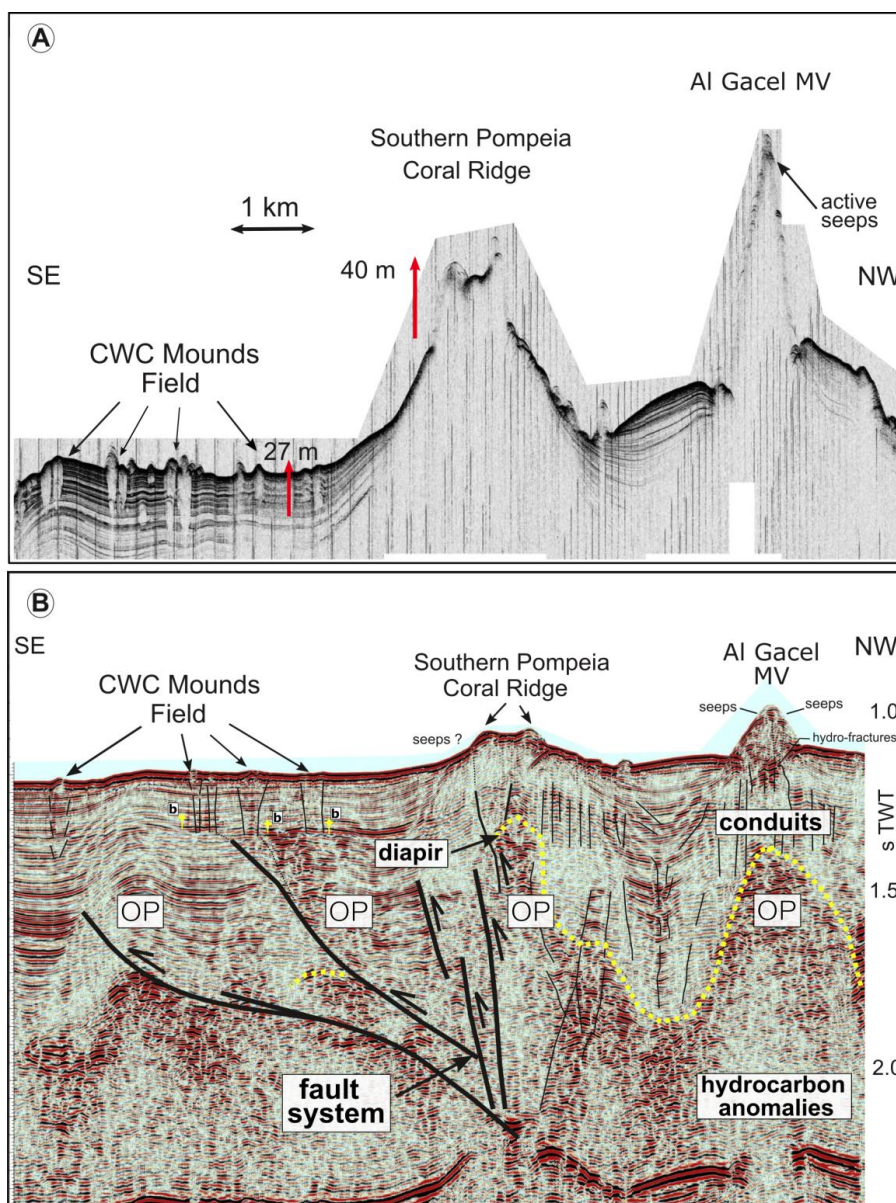
739



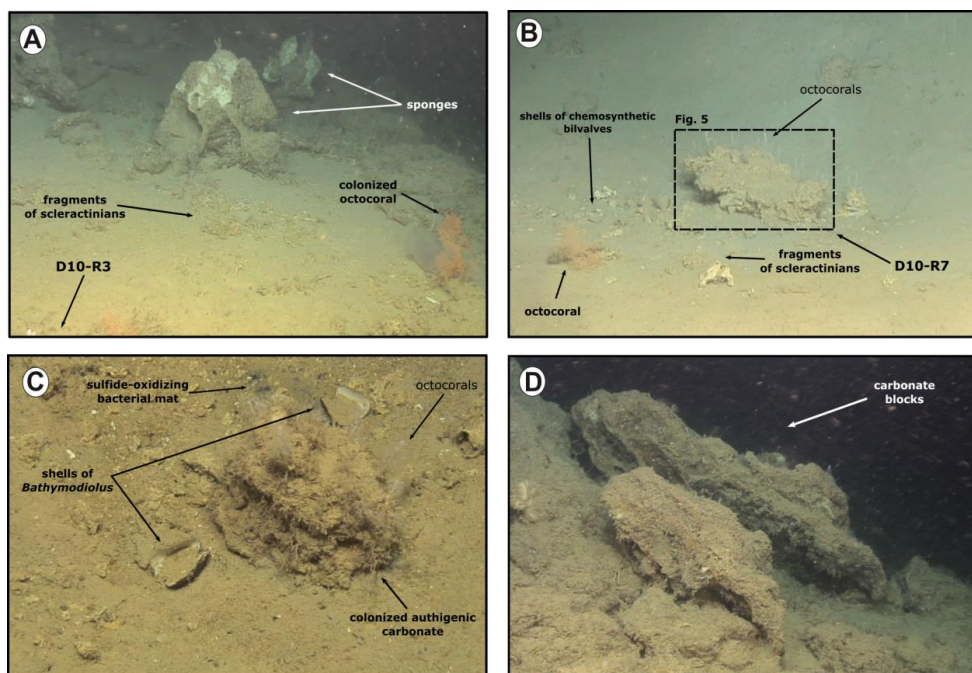
740
741 **Figure 1.** Bathymetric map of the study area. **A:** location of the Gulf of Cádiz between Spain, Portugal and
742 Morocco. The study area is marked with a red star; **B:** the Pompeia Province including its different morphological
743 features. Red lines indicate ROV-paths, yellow stars mark sampling sites; **C:** detailed map of the Al Gacel MV
744 including pathways of Dive 10 and 11 (black and blue lines, respectively). Further details of the area are provided
745 in **Figs. 2 and 3.**



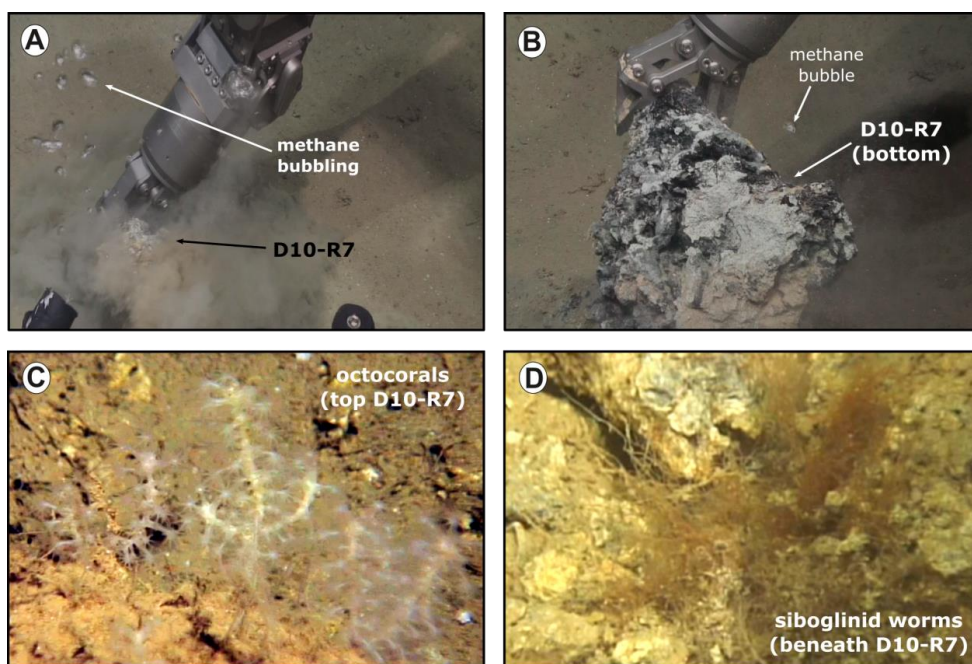
746
747 **Figure 2.** Bathymetric and seismic maps showing morphological features in the northern Pompeia Province. **A–**
748 **B:** bathymetric maps showing the Al Gacel MV, the Northern Pompeia Coral Ridge and the extinct MV. Yellow
749 stars mark sampling sites. **C:** seismic profile of the Pompeia Escarpment, westwards of the Northern Pompeia
750 Ridge.



751
 752 **Figure 3.** Seismic profiles showing geological features in the southern Pompeia Province. Note mud diapirism has
 753 been described in this area (Vandorpe et al., 2017). OP = overpressure zone.

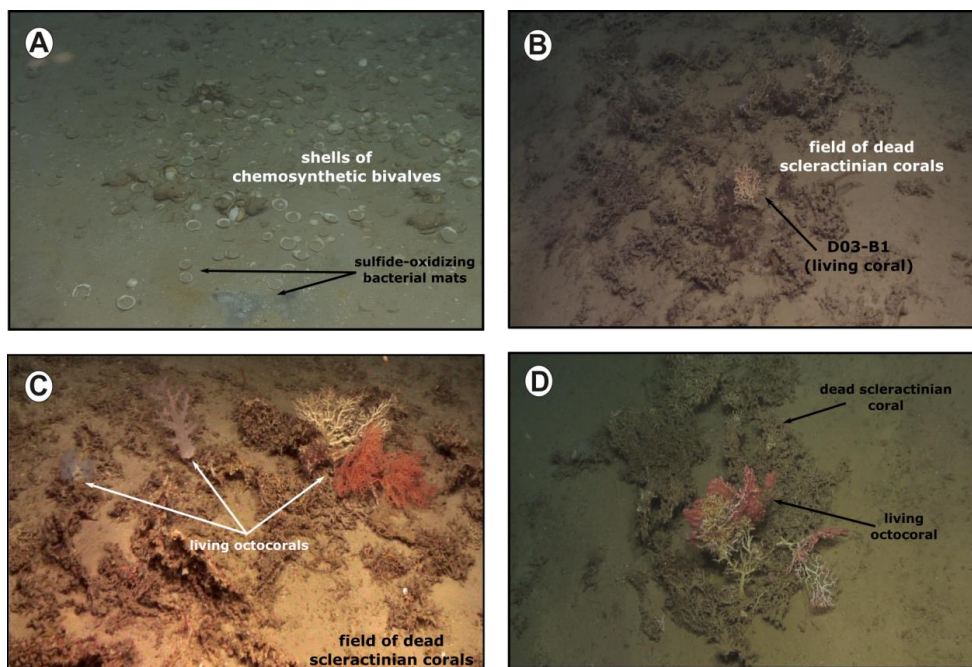


754
755 **Figure 4:** ROV still frames from the Al Gacel MV (Dives 10 and 11). **A:** eastern side of the volcano, displaying a
756 field of sponges, corals and carbonates; **B–C:** pockmark sites on the east side of the volcano, displaying authigenic
757 carbonate surrounded by shells of chemosynthetic bivalves, fragments of scleractinian and octocorals, as well as
758 sulfide-oxidizing bacterial mats; **D:** metric-sized carbonate blocks located in a slope at the summit of the volcano.
759
760



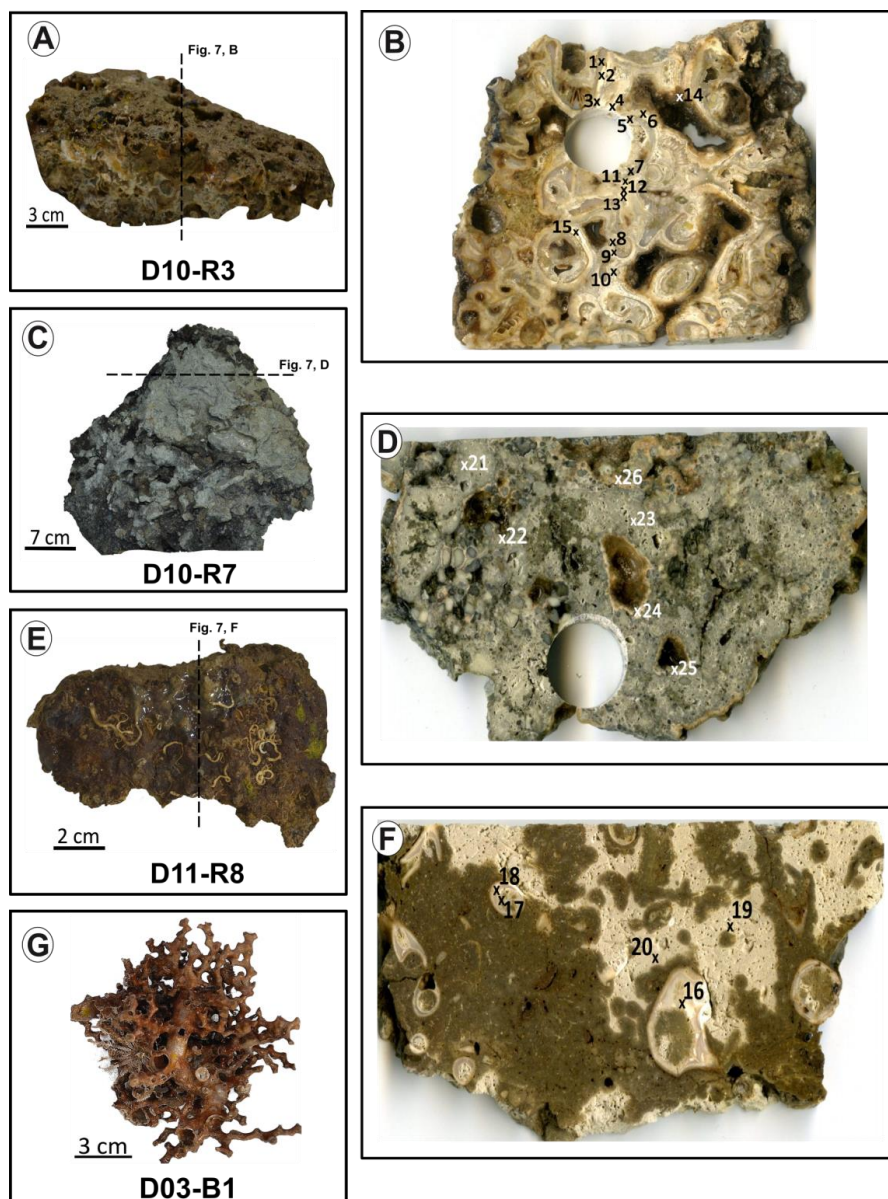
761
762
763
764
765
766
767

Figure 5: ROV still frames from the pockmark site shown in Fig. 4, B. **A–B:** release of bubbles while sampling; **C:** detailed photograph of the octocorals on top of the carbonate; **D:** detailed still frame from siboglinid worms beneath the carbonate.



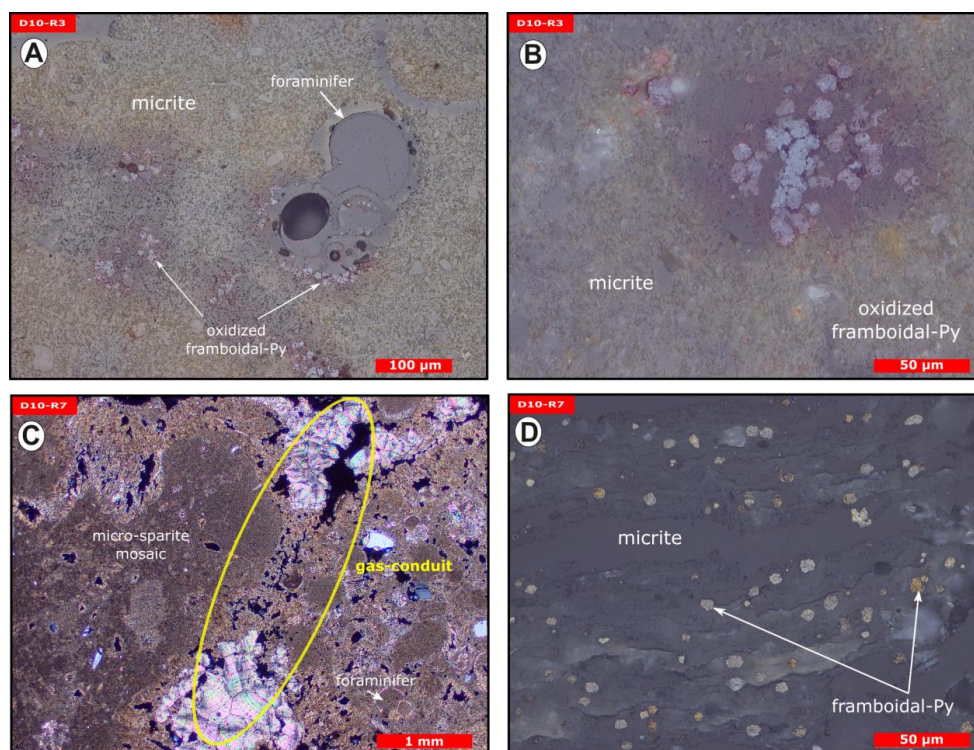
768
769
770
771
772

Figure 6. ROV still frames from the Northern Pompeia Coral Ridge and extinct MV (Dive 03). **A:** abundant shells of chemosynthetic bivalves with sulfide-oxidizing bacterial mats at the western site of the Northern Pompeia Coral Ridge; **B–D:** field of dead scleractinian-corals colonized by living corals; **D:** still frame from the extinct MV.

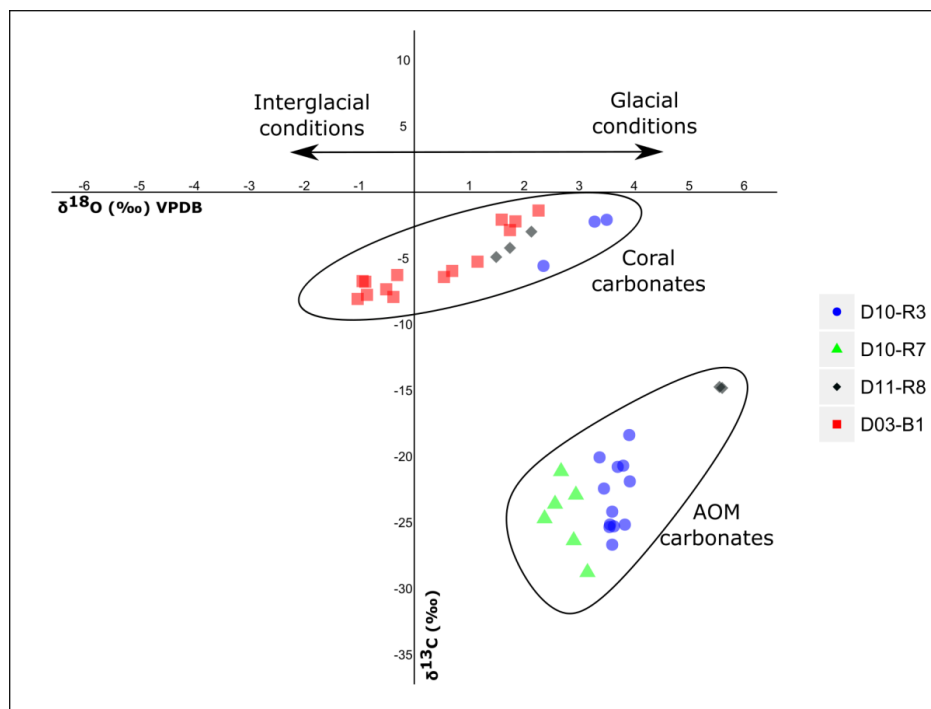


773
774 **Figure 7.** Photographs of analyzed samples including sampling sites for stable carbon and oxygen isotope ($\delta^{13}\text{C}$,
775 $\delta^{18}\text{O}$) analysis (crosses). **A–B:** D10-R3 carbonate with embedded corals; **C–D:** D10-R7 carbonate with strong H_2S
776 odor; **E–F:** D11-R8 carbonate with embedded corals; **G:** D03-B1 scleractinian-coral fragment, *Madrepora*
777 *oculata*.

778
779
780



781
782 **Figure 8.** Thin section photographs of MDACs. **A–B:** D10-R3 consisting of a micritic matrix with scattered
783 foraminifers and oxidized framboidal pyrites (reflected light); **C–D:** D10-R7 consisting of micritic and micro-
784 sparitic carbonate with abundant unaltered framboidal pyrites (C, transmitted light; D, reflected light). Please note
785 open voids which represent potential pathways for fluid seepage (yellow circle in C).
786



787

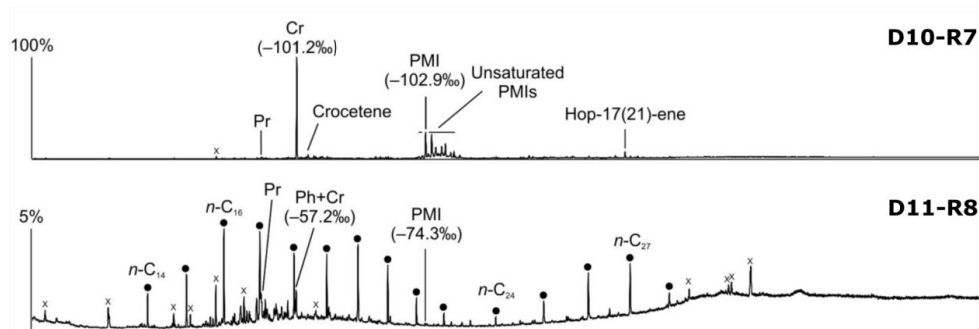
788 **Figure 9.** Stable carbon and oxygen isotopes ($\delta^{13}\text{C}$, $\delta^{18}\text{O}$) of samples from the Al Gacel MV and the Northern
789 Pompeia Coral Ridge (see **Figure 3** for precise sampling points).

790

791

792

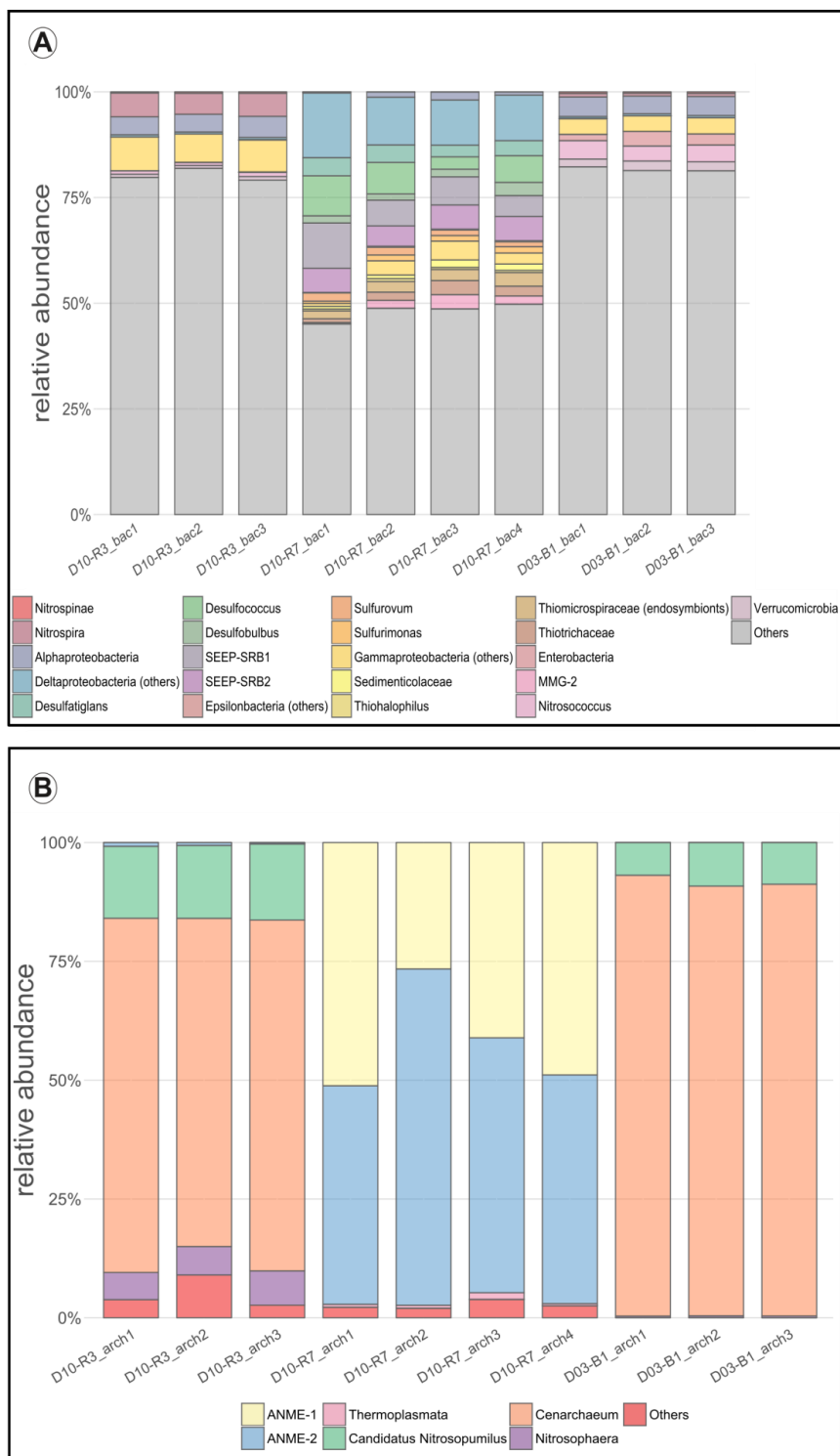
793



794

795 **Figure 10.** Total ion current (TIC) chromatograms of the analyzed samples. Isotopically depleted acyclic irregular
796 isoprenoids such as Cr and PMI are typically found in settings influenced by the anaerobic oxidation of methane
797 (AOM). Pr = pristane; Ph = phytane; Cr = crocetane; PMI = 2,6,10,15,19-pentamethylcosane; dots = n-alkanes;
798 crosses = siloxanes (septum or column bleeding). Percentage values given on the vertical axes of chromatograms
799 relate peak intensities to highest peak (Cr in D10-R7).

800





802 **Figure 11.** Bar chart representing the different taxa found in each sample according to relative abundances. A:
803 bacterial taxa; B: archaeal taxa. In “others” aggrupation is included taxa related to ubiquitous organism normally
804 found in sea- and seepage-related environments, and unclassified organisms. Number of reads per taxa detailed in
805 **Table S1** (bacteria) and **Table S2** (archaea).

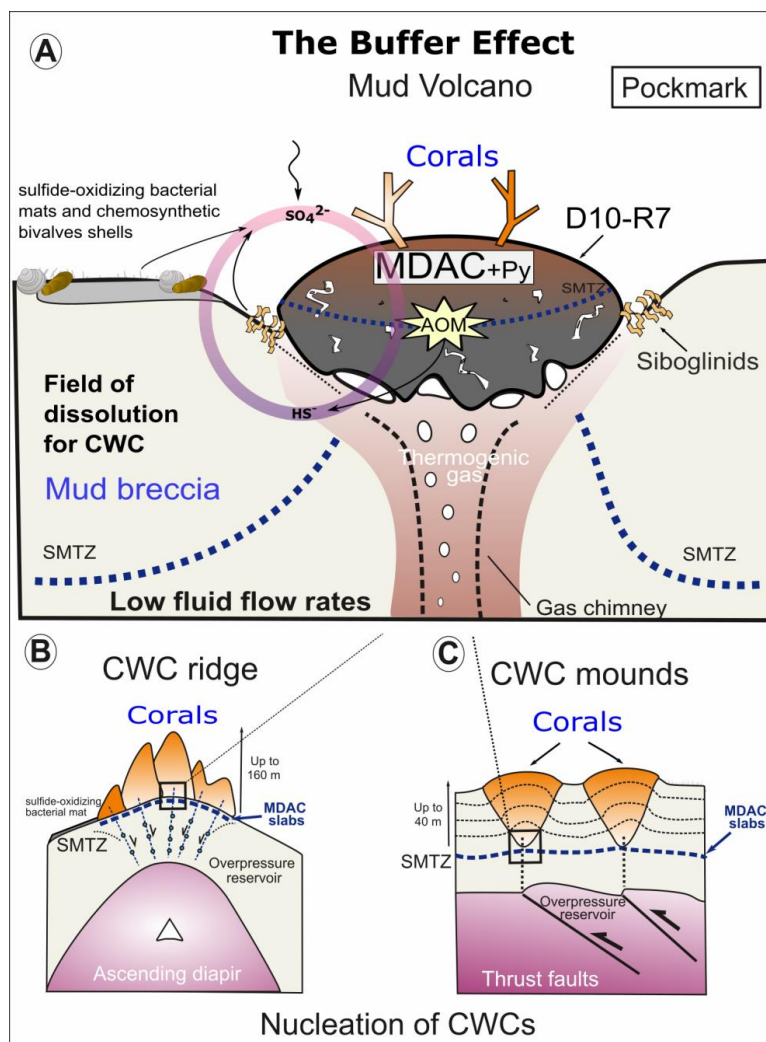


Figure 12. The buffer effect model. **A:** Buffer effect at pockmark sites (e.g. sampling site of D10-R7) where carbonates are formed directly on the bubbling site acting as a cap; **B:** Buffer effect at diapiric ridges where MDAC slabs are formed on the base of the ridge; **C:** Buffer effect at coral mounds where MDAC slabs are formed in deeper layers of the sediment. Py = pyrite, SMTZ: sulfur-methane transition zone.

810